Multi-stage subduction-related metasomatism recorded in whiteschists from the Dora-Maira Massif, Western Alps

Benedict J.R. Harris[1*], Jan C.M. De Hoog[1*], Ralf Halama[2], Hans-Peter Schertl[3] and Yi-Xiang Chen[4]

[1*]Grant Institute, School of GeoSciences, The University of Edinburgh, Edinburgh, EH9 3FE, United Kingdom.
[2]School of Geography, Geology and the Environment, Keele University, Keele ST5 5BG, United Kingdom.
[3]Institute of Geology, Mineralogy and Geophysics, Faculty of Geosciences, Ruhr-University Bochum, Bochum, 44780, Germany.
[4]CAS Key Laboratory of Crust-Mantle Materials and Environments, School of Earth and Space Sciences, University of Science and Technology of China, Hefei, 230026, China.

*Corresponding author(s). E-mail(s): b.j.r.harris@sms.ed.ac.uk; ceesjan.dehoog@ed.ac.uk;

Abstract

Whiteschists from the Dora-Maira massif (Western Alps, Italy) are Mg and K-rich metasomatised granites which experienced ultra-high pressure metamorphism and fluid-rock interaction during Alpine continental subduction. The sources and timing of fluid infiltration are a source of significant debate. In this study we present boron (B) isotopes and other fluid-mobile trace element (FME) concentrations in various generations of phengite from whiteschists and their country rock protoliths to investigate the sources and timing of metasomatic fluid influx. Reconstructed bulk rock concentrations based on modal data and mineral compositions indicate that significant amounts B and other FME were added to the rock during prograde metamorphism, but that this fluid influx postdates

the main Mg metasomatic event. High B concentrations (150–350 μg/g) and light $\boldsymbol{\delta^{11}B}$ values (-16 to -4 ‰) recorded in phengite point to a B-rich sediment-derived fluid as the main source of B in the whiteschists. Further redistribution of FME during metamorphism was associated with breakdown of hydrous minerals such as talc, phlogopite and ellenbergerite. The source of the Mg-rich fluids cannot be constrained based on the B data in phengite, since its signature was overprinted by the later main B metasomatic event. Rare tourmaline-bearing whiteschists record additional information about B processes. Tourmaline $\boldsymbol{\delta^{11}B}$ values (-6 to +1 ‰) are in isotopic equilibrium with similar fluids to those recorded in most phengite, but phengites in tourmaline-bearing samples records anomalous B isotope compositions that reflect later redistribution of B. This study demonstrates the utility of *in situ* analyses in unravelling complex fluid-rock interaction histories, where whole rock analyses make it difficult to distinguish between different stages of fluid-rock interaction. Polymetasomatism may result in decoupling of different isotopic systems, thus complicating their interpretation. The Dora-Maira whiteschists interacted with multiple generations of fluids during subduction and therefore may represent a long-lived fluid pathway.

Keywords: whiteschist, boron isotopes, ultra-high pressure metamorphism, fluid-rock interaction, subduction metasomatism

Introduction

High pressure fluids are important agents for the transfer of fluid-mobile trace elements within the subducting slab and to the mantle wedge. (Ultra-)high pressure rocks (UHP) provide a record of the generation of such fluids and of the mobilization of trace elements within the slab. Two approaches exist to recover (U)HP fluid compositions. Analysis of fluid inclusions trapped in (U)HP minerals provides direct constraints on fluid compositions (e.g. Ferrando et al., 2009; Philippot et al., 1995; Maffeis et al., 2021; Hughes et al., 2021), but are often rare and volumetrically small, which hampers their analysis. Alternatively, whole rock or mineral elemental and isotopic compositions, combined with fluid-rock partitioning data provides an indirect method of constraining fluid compositions, and is applicable to a wider range of rocks (e.g. Konrad-Schmolke and Halama, 2014; Halama et al., 2020; Busigny et al., 2003; Tian et al., 2019; Harris et al., 2022). *In situ* analyses of multiple fluid-mobile elements and isotope systems are particularly powerful for investigating the evolution of mineral and coexisting fluids during progressive stages of metamorphism and fluid-rock interaction (e.g. Urann et al., 2020; Halama et al., 2020; Debret et al., 2016; Bebout et al., 2007; De Hoog et al., 2014; Clarke et al., 2020; Harris et al., 2022).

The Dora-Maira whiteschists are continental rocks metamorphosed at UHP conditions during Alpine subduction of the European continental margin beneath the Adriatic Plate. They are characterized by extreme enrichment in Mg, and depletion in Na, Ca, Fe, and LILE relative to their country rocks (Schertl and Schreyer, 2008; Schertl et al., 1991; Chopin, 1984). They have been extensively studied after they revealed the first record of coesite in crustal rocks, indicating subduction to depths of at least 100 km (Chopin, 1984). The

whiteschists represent a former fluid pathway which was active during continental subduction (Ferrando et al., 2009; Chen et al., 2016; Xiong et al., 2021, 2022; Tian et al., 2019; Chen et al., 2023). Chopin (1984) originally suggested an evaporitic protolith for the whiteschist. Most authors now regard the whiteschists as metasomatic alteration products of the orthogneiss and metagranite country rock by Mg-rich fluids (e.g. Schertl and Schreyer, 2008; Gebauer et al., 1997; Ferrando et al., 2009) but there is outstanding debate over the timing of metasomatic event(s) and the origin of metasomatic fluid(s). Oxygen and hydrogen isotope data have been used to argue that the metasomatic fluid was seawater-derived but this has been interpreted as a signature of both pre-Alpine seafloor hydrothermal alteration (Gauthiez-Putallaz et al., 2016) and Alpine prograde dehydration of serpentinites (Chen et al., 2016) or altered oceanic crust (AOC) (Sharp et al., 1993). Gauthiez-Putallaz et al. (2016) proposed that Mg-metasomatism occurred on the seafloor where the Dora-Maira crust formed part of a hyper-extended continental margin sequence. Similar explanations have been proposed for whiteschists from the Monte Rosa nappe (Pawlig and Baumgartner, 2001; Marger et al., 2019). Compagnoni and Hirajima (2001) documented rare 'superzoned' garnet with almandine-rich cores and pyrope-rich rims. The extreme compositional zoning shown is interpreted to be produced by a change in the whole rock bulk composition. Based on the inclusion assemblage in the almandine-cores they estimated the P-T conditions of formation to be $\sim$ 1.6 GPa and 600 °C and concluded that subsequent Mg-metasomatism took place during Alpine subduction.

In this study we examine the mobility of trace elements during metasomatism and (U)HP metamorphic reactions. We combine *in situ* SIMS analyses of fluid-mobile elements (FME) and boron (B) isotopes in protolith and metasomatic minerals to address three main questions. 1) What were the sources

of metasomatic fluids which interacted with the granitic rocks to produce whiteschist during subduction? 2) Do the unusual major element, trace element, and isotopic signatures all record interaction with the same fluid, or were there multiple periods of fluid influx? 3) To what extent was trace element distribution between minerals at different stages of metamorphism controlled by internal metamorphic reactions versus external fluid input? Boron isotopes are particularly suited to address the first two questions, since different subducted lithologies have distinct B isotope signatures (De Hoog and Savov, 2018).

Geological background

The Dora-Maira massif (DMM) forms one of the three Internal Crystalline Massifs within the Pennine Domain of the Western Alps (Chopin, 1984; Compagnoni and Hirajima, 2001) and exposes part of the European continental margin that was subducted and exhumed during the Alpine orogeny. It is now stacked within the Western Alps orogenic wedge, where it forms a dome roofed by normal-sense shear zones, which juxtapose the Monviso massif, and other units of the oceanic Piedmont zone (Lardeaux et al., 2006). The internal structure of the DMM consists of multiple thrust sheets, which experienced different peak pressure-temperature conditions during Alpine metamorphism (Figure 1). The Brossasco-Isasca Unit (BIU) in the southern DMM experienced peak UHP Alpine metamorphism at 730 °C, 4.0–4.3 GPa (Groppo et al. (2019) and references therein) and is divided into a polymetamorphic complex and a monometamorphic complex (Compagnoni et al., 1994). The polymetamorphic complex comprises almandine-kyanite-phengite metapelite with subordinate marble and eclogite, and represents Variscan metamorphic basement, with partial Alpine HP metamorphic overprinting. The monometamorphic complex comprises garnet-biotite-phengite orthogneiss, with local

occurrences of whiteschist lenses, garnet-jadeite quarzite, undeformed metagranite, and metapelite. This complex is interpreted as recording Permian granitoids intruded into the Variscan basement (Gebauer et al., 1997; Chen et al., 2017) and subsequently metamorphosed and deformed during Alpine subduction. The metapelite inclusions in orthogneiss are interpreted as xenoliths of the country rock (Compagnoni and Hirajima, 2001). Whiteschist is a term introduced by Schreyer (1973) to describe magnesian rocks containing the high pressure assemblage talc + kyanite, with a bulk composition characterized by extremely high Mg/Fe ratio, very low Ca and Na, and high Al contents. In the BIU the whiteschists contain pyrope-rich garnets ($X_{Prp} > 0.9$) and have also been referred to as pyrope-quartzites in the literature (Chopin, 1984). The BIU whiteschists occur as decametric lenses within otherwise unremarkable orthogneiss. The contact between the lithologies is typically marked by alteration in the whiteschist. Whiteschists preserve an internal foliation which is truncated by the external foliation in the orthogneiss (Schertl et al., 1991), implying that they record a different stage of the BIU metamorphic and structural evolution.

The petrography of the whiteschists has been described in detail by Schertl et al. (1991). The matrix is mineralogically simple and consists of pyrope garnet, phengite, quartz (retrograde after coesite), kyanite, rutile, ± talc ± jadeite. Small pyrope and kyanite porpyroblasts contain inclusions of quartz, relict coesite, phengite, talc, rutile ± tourmaline. The presence of coesite was first described by Chopin (1984) and confirms the UHP conditions experienced by the BIU. Decimetric pyrope megablasts consist of a core with a diverse inclusion assemblage, including several phases which do not occur in the matrix or small pyropes. These include Mg-chlorite, ellenbergerite, phlogopite and vermiculite, alongside kyanite and talc, which also occur in the matrix. Glaucophane,

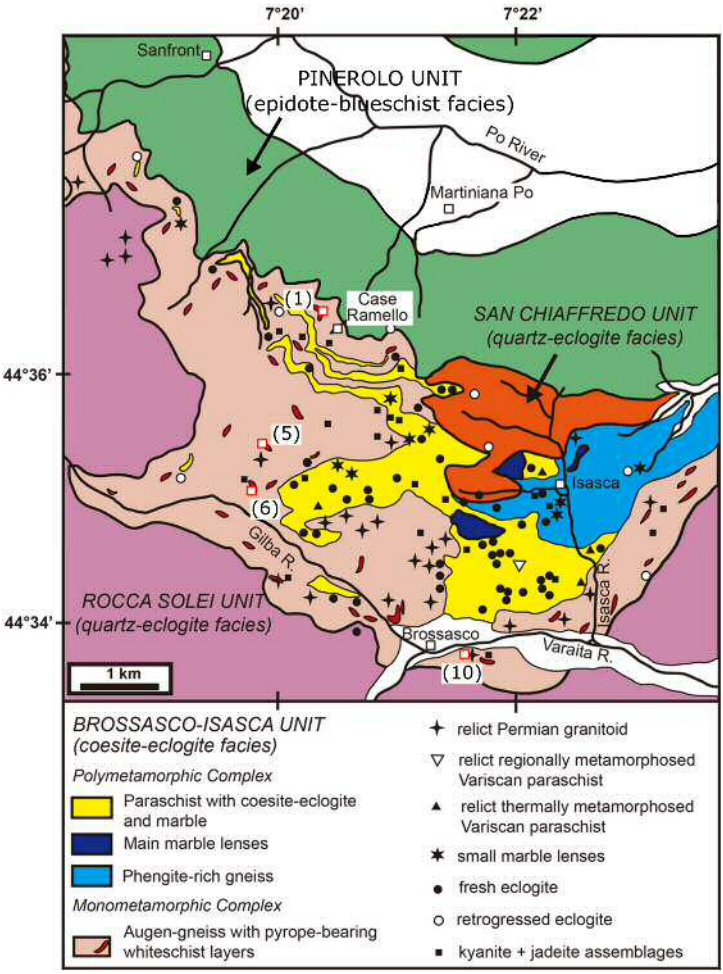

Figure 1 Geological map of the southern Dora-Maira Massif, showing sample localities, with locality numbers following Schertl and Schreyer (2008). (1) DM5.2, DM6, DM1.1, 15597, 17478, 21437; (5) 20178, DM1b, 26405 (nearby) (6) 17618; (10) 17702. Modified after Chen et al. (2016), originally after Compagnoni and Rolfo (2003).

paragonite, muscovite, tourmaline, apatite, bearthite and Mg-dumortierite are rare inclusion phases. Magnesiochloritoid has also been found in megablasts from the Tapina locality (Simon et al., 1997). Quartz/coesite is absent from the megablast cores and phengite is extremely rare. Some megablasts contain a thin rim with similar composition and inclusion assemblage to the small pyropes. Occasionally various phengite schists occur, which are intercalated

with the whiteschists (Schertl and Schreyer, 2008). These phengite schists have bulk compositions intermediate between the country rock orthogneiss and the whiteschists, and contain phengite, quartz ± phlogopite ± chlorite ± garnet ± kyanite ± tourmaline ± jadeite.

The Alpine P-T path of the BIU has been constructed from P-T estimates in multiple different lithologies (Figure 2). The earliest recorded stage of Alpine metamorphism is the growth of garnet cores in metapelites at 520–540 °C, 1.6–2.3 GPa (Groppo et al., 2019). Garnet mantles record slightly higher grade conditions (540–560 °C, 2.5–2.8 GPa), similar to the conditions suggested by Ferrando et al. (2009) for pyrope megablasts hosting ellenbergerite in whiteschists. Similar pressure estimates have also been recovered from phengite cores in marbles (Di Vincenzo et al., 2006). Growth zoning in clinopyroxene, garnet and phengite in eclogites records a similar prograde path (540–500 °C, 1.5 GPa; 570 °C, 2.5 GPa; 650 °C, 3.2 GPa; Nowlan et al. (2000)). The peak metamorphic conditions (∼ 730 °C, 4.0–4.3 GPa) are well studied, with the best constrained estimates coming from metapelite garnet rims (Groppo et al., 2019), whiteschists (Hermann, 2003), and marbles (Castelli et al., 2007). Early retrograde decompression is recorded by phengite-talc-kyanite coronae in whiteschists (∼ 720 °C, 3.6–3.9 GPa, Hermann (2003)). Further decompression and cooling (670–700 °C, 2.5–3.0 GPa) is recorded by phengite-phlogopite-talc-kyanite coronae in whiteschists (Hermann, 2003) and retrograde assemblages in eclogites (Groppo et al., 2007; Di Vincenzo et al., 2006), and marbles (Castelli et al., 2007). A major retrograde event, in response to a fluid influx, occurred at 600–650 °C, 1.1–1.5 GPa and is recorded by near-complete recrystallization in the orthogneiss (Di Vincenzo et al., 2006; Groppo et al., 2005), complete retrogression of pyrope in some whiteschists (Hermann, 2003), and also by assemblages in metapelites (Groppo et al., 2019), marbles (Groppo et al., 2007)

and eclogites (Di Vincenzo et al., 2006; Groppo et al., 2007). Even lower grade assemblages ($\sim$ 550 °C, 0.5–1.0 GPa) are preserved in calc silicates (Rubatto and Hermann, 2001).

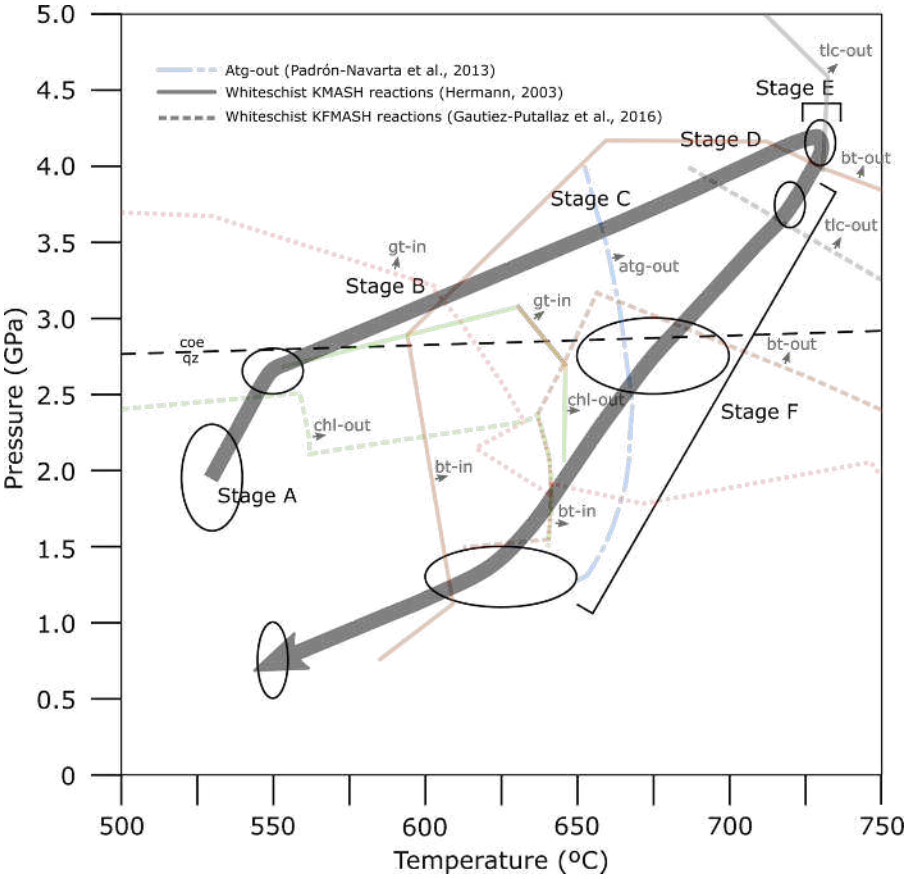

Figure 2 Summary of P-T path constrained from metapelite (Groppo et al., 2019; Compagnoni and Hirajima, 2001; Hermann, 2003), eclogite (Di Vincenzo et al., 2006; Groppo et al., 2007; Hermann, 2003; Nowlan et al., 2000), whiteschist (Compagnoni and Hirajima, 2001; Ferrando et al., 2009; Ferraris et al., 2005; Gauthiez-Putallaz et al., 2016; Hermann, 2003), marble (Ferrando et al., 2017; Di Vincenzo et al., 2006; Castelli et al., 2007; Groppo et al., 2007), calc silicate (Rubatto and Hermann, 2001) and orthogneiss (Di Vincenzo et al., 2006). Ellipses represent the uncertainty on P-T estimates for each point (see Geological background section). Stages, indicated by capital letters, correspond to stages of the whiteschist mineralogical evolution and are discussed later. Key mineral growth and breakdown reactions in the whiteschists (see discussion) are shown in the K_2O–MgO–Al_2O_3–SiO_2–H_2O (Hermann, 2003) and K_2O–FeO–MgO–Al_2O_3–SiO_2–H_2O (Gauthiez-Putallaz et al., 2016) systems. Also shown is the breakdown of antigorite (Padrón-Navarta et al., 2013), which has been proposed as a source of Mg-rich fluids. Mineral abbreviations after Whitney and Evans (2010)

Analytical techniques

Mineral major element compositions were determined using a Cameca SX100 electron microprobe equipped with 5 wavelength dispersive spectrometers at the School of Geosciences, University of Edinburgh, UK. Acceleration voltage was 15 kV, beam current was 4 nA for major elements and 100 nA for minor elements. Beam diameter was 2 μm for anhydrous minerals and 5 μm for hydrous minerals. On-peak counting times (seconds) were as follows (background time in brackets). Major elements: K 20 (10), Na 20 (10), Ca 20 (10), Mg 20 (10), Fe, Si 20 (10), Al 20 (10). Minor elements: K 20 (10), Na 20 (10), Ca 50 (25), Mg 20 (10), Ti 60 (30), Mn 80 (40), P 20 (10), Zr 60 (30). A variety of synthetic and natural standards were used for calibration.

Selected trace elements and B isotopes in minerals were measured in situ by Secondary Ion Mass Spectrometry (SIMS) at the Edinburgh Ion Microprobe Facility, School of Geosciences, University of Edinburgh, UK, using a Cameca 7f-Geo equipped with a Hyperion RF oxygen source. Full data are provided in Online Resource 2. Boron isotopes in minerals other than tourmaline were measured by sputtering the sample surface using a 20 nA $^{16}O^-$ primary beam in Kohler illumination mode and extracting the sputtered ions into the mass spectrometer. The analytical spot was about 25 μm wide. A single electron multiplier was used to count $^{10}B^+$, $^{11}B^+$ and $^{28}Si^{2+}$ signals sequentially for 8, 2 and 1 s, respectively, with 50 repeat cycles comprising a single analysis. Centering of the secondary beam relative to the field aperture and centering of the reference peak mass ($^{28}Si^{2+}$) were done in an automated routine prior to each analysis. A mass resolution of 1500 (M/ ΔM) was used to avoid ^{9}BeH and ^{10}BH interference peaks. Boron isotope ratios were corrected for instrumental mass fractionation using Phe80-3 phengite ($\delta^{11}B$ = -13.5 ‰; Pabst et al. (2012)). In addition, B6 obsidian, ARM-1 andesite glass and GB4 obsidian were measured

to monitor drift and relative offset of phengite compared to glass standards, which was -3 ‰ using values compiled in GeoReM. Reproducibility of the glass standards was 0.4–0.7 ‰ (1sd) whereas reproducibility of Phe80-3 was 1.6 ‰ (1sd, n=23), which suggests some minor heterogeneity of the Phe80-3 material. In addition, muscovite 98973 was measured as a secondary standard. Two rather different bulk values exist in the literature (-8.8 ± 0.3 ‰Dyar et al. (2001) vs -20.00 ± 0.36 ‰Codeço et al. (2019)). The origin of this discrepancy is unknown, but we note that concentration of B and several other elements are heterogeneous and different from reported values (Harris et al., 2022), suggesting further evaluation of this material is needed. We obtained a δ^{11}B value of -20.2 ± 0.3 ‰ (1se, n=12), which closely matches the value reported by Codeço et al. (2019) from bulk MC-ICP-MS analysis. Finally, mica MVE02-8-5 and JJE01-X-3 (Martin et al., 2015) were also measured, but both minerals are extremely heterogeneous exhibiting nearly 20 ‰ variations and are therefore less suitable as calibration materials.

Boron isotopes in tourmaline were measured using a similar setup except for using a ca. 100 nA beam, counting times of 4, 2 and 0.5 s for ^{10}B, ^{11}B and ^{30}Si, respectively, in 20 cycles and using a single Faraday Cup detector. Spot size was ca. 25 μm. Tourmaline dravite 108796 (our value -6.7 ± 0.5 ‰, reference value -6.6 ± 0.2 ‰), elbaite 98144 (our value -11.1 ± 0.4 ‰, reference value -10.5 ± 0.4 ‰) and schorl 112566 (our value -11.7 ± 0.3 ‰, reference value -12.5 ± 0.1 ‰) were used for calibration (Dyar et al., 2001). Small average offsets of 0.7–0.9 ‰ were measured for the latter two standards compared to the first, indicating a small matrix effect. As the analysed tourmalines were close to dravite this will have negligible effect on their accuracy. Typical internal precision was 0.1 ‰ (1s), whereas repeatability of standards was 0.3–0.5 ‰. Our mean tourmaline boron isotope values for each sample matched

from those of Xiong et al. (2022), measured by LA-MC-ICP-MS, within 1 ‰, which is well within the range of values within each sample (Online Resource 2).

Trace element contents of various minerals were measured using a similar setup as B isotope analysis of the same minerals, but using a lower mass resolution of 600 to increase transmission and a beam current of 5 nA to reduce spot size to ca. 15 μm. A variety of glass and mica standards were used for calibration, which is particularly important for halogens which experience strong matrix effects and accuracy benefits from matrix-matched standards. GSD1-G was used as the main calibration standard for elements other than halogens with preferred values from GeoReM (Jochum and Stoll, 2008), except B for which we adopted a value of 65 μg/g, following Walowski et al. (2019). Nitrogen was measured in a separate routine as detailed in Harris et al. (2022).

Sample descriptions and major element compositions

A total of eleven samples were analysed (Table 1). Samples with five digit numbers (e.g. 17702) have been previously described (Schertl and Schreyer, 2008; Xiong et al., 2022), whereas other samples are new (DMxx). Sample locations (Figure 1) follow the numbering of Schertl and Schreyer (2008). A description of each lithology is provided below. Detailed mineralogy of each sample is provided in Table 1, representative major element compositions are presented in Online Resource 1, and selected photomicrographs of the samples are shown in Figure 3.

The whiteschist and phengite schist protoliths are represented by the metagranite (sample 17702) and orthogneiss (sample 20178). In the metagranite, randomly oriented K-feldspar occurs as large grains up to 2 cm in length.

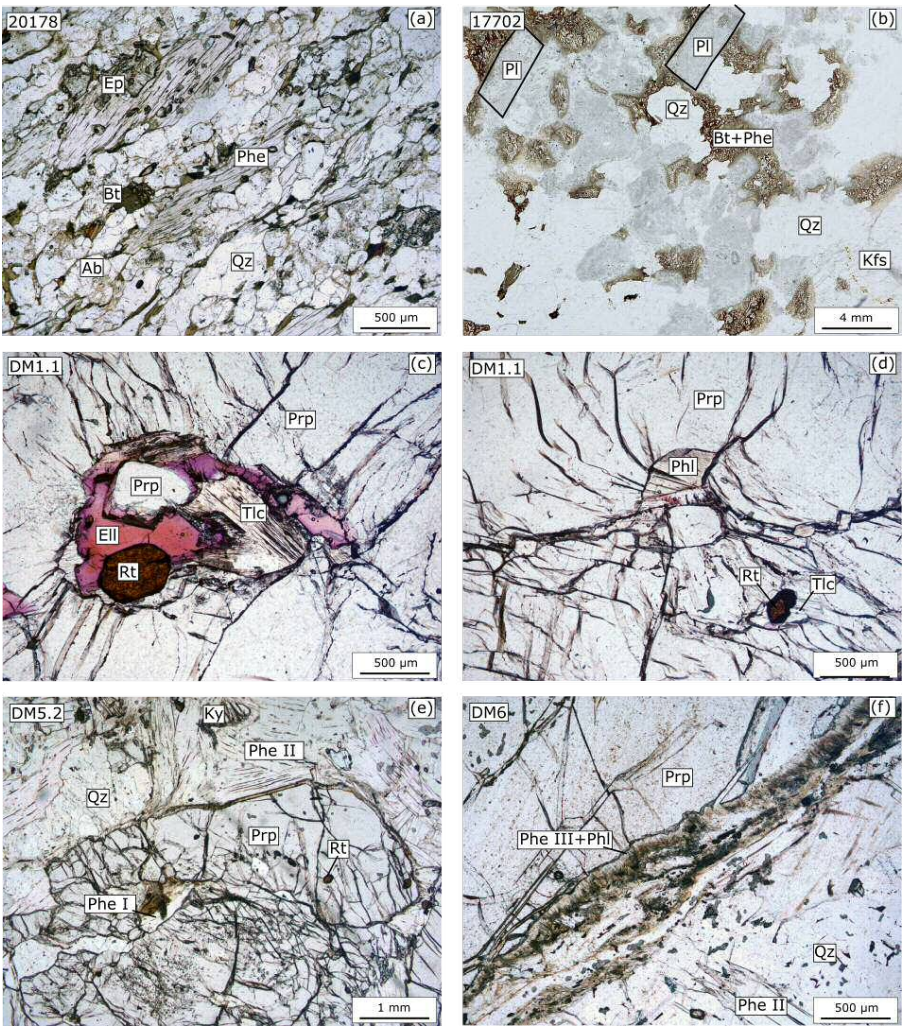

Figure 3 Thin section photomicrographs of metagranite, orthogneiss and whiteschist. All images are in plane polarized light. (a) Orthgneiss sample 20178, showing the amphibolite facies assemblage epidote, biotite, albite, phengite and quartz. (b) Metagranite sample 17702. Igneous K-feldspar is largely unaffected by high pressure metamorphism. Quartz is also largely unreacted, but is recrystallized into granoblastic, polygonal grains. Red-brown igneous biotite is partially replaced by colourless phengite. Plagioclase laths are pseudomorphed by a fine-grained aggregate of zoisite, jadeite, quartz and phengite. (c) Whiteschist sample DM1.1, showing a composite inclusion of ellenbergerite, talc and rutile in a pyrope megablast (Prp I). (d) Whiteschist sample DM1.1, showing inclusions of phlogopite, talc and rutile in a pyrope megablast (Prp I). (e) Whiteschist sample DM5.2, showing a small pyrope (Prp II) with inclusions of phengite (Phe I) and rutile. (f) Whiteschist sample DM6, showing Phe III + phlogopite forming at the expense of pyrope on the rim of pyrope megablasts. Mineral abbreviations after Whitney and Evans (2010).

Sample	Lithology	Locality name	Locality number	Mineralogy
17702	Metagranite	Brossasco	10	Qz, Kfs, Pl, Phe, Bt, Grt, Zo, Jd, Ky
20178	Orthogneiss	Tapina	5	Qz, Ab, Bt, Phe, Grt, Ep, Rt, Ttn
DM1.1	Pyrope megablast	Case Ramello	1	Prp, Chl, Ell, Phl, Ky, Tlc
DM5.2	Whiteschist	Case Ramello	1	Phe, Prp, Qz, Ky, Tlc, Rt
DM6	Whiteschist	Case Ramello	1	Phe, Prp, Qz, Coe, Ky, Tlc, Rt, Ell
15597	Whiteschist	Case Ramello	1	Phe, Prp, Qz, Ky, Tlc, Rt, Tur, Jd
DM1b	Whiteschist	Tapina	5	Phe, Prp, Qz, Ky, Tlc
17478	Retrogressed whiteschist	Case Ramello	1	Qz, Chl, Ms, Phe, Tlc, Ky, Tur
21437	Phengite schist	Case Ramello	1	Phe, Qz, Tur, Chl, Grt
26405	Phengite schist	San Bernardo	near 5	Phe, Qz, Phl, Tur, Grt, Ky, Rt
17618	Phengite schist	Masueria	6	Phe, Ms, Pg, Phl, Chl, Tlc, Tur, Grt, Rt

Table 1 Summary of sample information. Locality numbers and names follow Schertl and Schreyer (2008). Mineral abbreviations after Whitney and Evans (2010).

Quartz occurs in patches up to 1 cm, which are composed of granoblastic, polygonal grains about 0.2 mm in diameter. This texture has previously been interpreted to reflect the former presence of coesite (Biino and Compagnoni, 1992). Biotite (6.01 Si pfu [22 O pfu], X_{Mg}=0.40) is present, but is partially replaced by Ti-rich phengite ($TiO_2 > 1.5$ wt%), which was interpreted as forming during prograde HP metamorphism (Bruno et al., 2001). Rectangular plagioclase laths are pseudomorphically replaced by a fine grained aggregate containing zoisite, jadeite, quartz and a Ti-poor phengite ($TiO_2 < 0.4$ wt%).

In the orthogneiss, phengite occurs as large, oriented grains up to 1 mm in length and also as a separate generation of smaller flakes, which along with biotite define the foliation. Epidote, albite and titanite are also weakly aligned in the direction of the foliation. The biotite-epidote-phengite-albite-titanite assemblage was previously interpreted to have crystallized at amphibolite facies ($\sim$ 1.0–1.5 GPa, 600–650 °C) on the retrograde path (Groppo et al., 2005). Garnet occurs as anhedral grains with a black oxide rim, suggesting that it is out of equilibrium with other minerals. Sharp et al. (1993) calculated temperatures of 700–750 °C from oxygen isotope thermometry of garnet–quartz–rutile in orthogneiss samples, similar to the peak temperatures recorded in whiteschists, suggesting that garnet and rutile represent relict UHP phases. No oxygen isotope data were available for phengite, but the cores of large

phengites preserve high Si contents (6.97 ± 0.04 Si pfu), which are suggestive of HP metamorphism. Biotite was out of oxygen isotopic equilibrium with the garnet-quartz-rutile assemblage, which is consistent with it forming during retrogression (Sharp et al., 1993).

Whiteschists consist of a matrix containing quartz, phengite, kyanite and rutile ± jadeite ± tourmaline ± monazite ± zircon. Within the matrix there are large pyrope megablasts (up to 10 cm diameter) and small pyrope porphyroblasts (0.5–1 cm). Pyrope megablasts in our samples display two zones with differing garnet composition and inclusion assemblages. The cores (Prp I, $Prp_{92-97}Alm_{2-6}Grs_{1-2}$) contain inclusions of kyanite, talc, rutile, ellenbergerite, phlogopite and sometimes Mg-chlorite (sample DM1.1). The phlogopite is K-deficient and similar to that identified by Schertl et al. (1991). Ellenbergerite shows large compositional variation (0–4.3 wt% TiO_2, 0–2.2 wt% ZrO_2, 0–12.6 wt% P_2O_5) associated with the substitutions Si + Al → P + Mg and (Ti,Zr) + Mg → 2Al (Chopin et al., 1986). The megablast rims (Prp II) are almost entirely free of Ca and contain inclusions of phengite, coesite, quartz (after coesite), kyanite, talc, rutile and occasionally tourmaline (sample 15597). Small pyropes (Prp II, $Prp_{87-93}Alm_{6-12}Grs_1$) contain the same inclusion assemblage as the pyrope megablast rims. The outermost rim of the pyrope megablasts is replaced by fibrous phengite and phlogopite. Three generations of phengite are recognisable in the whiteschist: inclusions in Prp II (phengite I), matrix phengite (phengite II), breakdown products on pyrope rims (phengite III). Mean Si contents are very similar in Phe I (7.15 ± 0.06 pfu [22 O pfu]) and II (7.14 ± 0.04 pfu) and slightly lower in Phe III (7.10 ± 0.05 pfu) but all three populations overlap significantly (Figure 4). $Mg/(Mg+Fe^{2+})$ is >0.85 in all whiteschist minerals, consistent with the high bulk rock value. Our petrographic observations fit with the previously

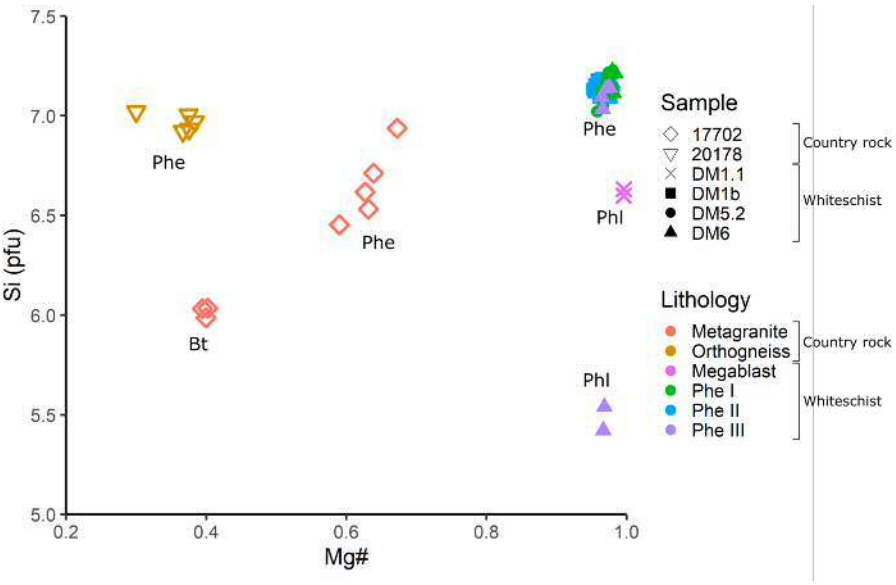

Figure 4 Si (pfu) and Mg number ($Mg/(Mg+Fe^{2+})$) in white mica and biotite. Colours represent the textural affinity of each analysis. For example, Phe III includes phengite as well as the associated phlogopite (see text for details, [Sample descriptions and major element compositions]

described phase evolution of the whiteschists (e.g. Schertl et al., 1991; Ferrando et al., 2009). Tourmaline occurs only in rare samples (Table 1), which were described in detail by Xiong et al. (2022). Tourmaline in these samples occurs only in the matrix and as inclusions in Prp II, alongside coesite/quartz, phengite, talc and kyanite.

Phengite schists are mineralogically variable but all contain significant amounts of phengite and quartz. Samples in this study also contain tourmaline and were described by Xiong et al. (2022). Other minerals present in the matrix include chlorite, phlogopite, muscovite, paragonite, garnet, kyanite and talc.

Sample	Textural position	Mineral	n	N	Li	B	Be	Rb	Sr	Cs	F	Cl	H_2O (wt%)
17702	Replacing Bt	Phe	5	72	547	64	16	1291	8.5	67	2909		3.7
	Replacing Pl	Phe	2		404	205	5.7	431	28	10	2017		4.2
	Igneous	Kfs	4		6.1	6.1	1.4	384	231	6.9	8.1		
	Igneous	Bt	4		914	2.5	7.3	1278	2.2	99	6199		
20178	Matrix	Phe	14	41*	160	277	17	586	9.9	9.2	1683	80	3.9
		Bt	2		646	1.2	4.6	1005	25	52	4600	1163	
		Ep	1	5	0.20	2.6	3.6	0.58	757	1	184		
		Ab	1	0.7	0.04	3.6	3.2	0.8	17	0.8	2.8		
DM1.1	Megablast core	Phl	2		11	50	2.9	172	15	19	5695	352	4.8
		Tlc	2		0.17	8.0	0.07	0.1	0.15	0.01	1316	601	3.8
		Ell	9		0.38	21	6.1	0.04	0.07	0.16	262	138	6.9
DM6	Megablast core	Ell	2		0.04	8.4	7.1	<0.01	0.11	2.2	130	84	6.1
	Megablast mantle	Ell	2		0.34	6.7	4.2	0.03	0.10	0.38	290	384	6.1
		Tlc	1	3.4	1.4	0.92	0.02	0.32	0.07	<0.01	3597	82	3.6
		Grt											
	Matrix pyrope	Grt	1.0	1.2	11	0.24					34		
	Megablast rim/ matrix pyrope	Phe I	5	39	71	272*	11	414	21	4.2	1389*	21	4.0
	Matrix	Phe II	9	29	68	188	11	390	17	3.5	2178	82	3.8
	Retrograded megablast rim	Phe III	5	208	53	196	11	409	20	3.8	1407	120	3.6
		Phl	1		65	33	3.0	67	1.7	0.81	8360		4.1
		Grt											
DM5.2	Matrix pyrope	Grt	2		9.9	0.27	<0.01	0.17	0.02	0.06	55		
		Phe I	10		54	231	11	388	19	3.7	1658		3.9
		Tlc	1		0.25	6.2	0.08	0.24	0.23	0.01	2905		3.4
	Matrix	Phe II	12		68*	193*	11	372	19	3.4	2296		3.9
DM1b	Matrix pyrope	Grt	1	0.61	14	1.1					41		
	Matrix	Phe II	16	17	45	358	9.7	339	12	5.5	2411	54	
	Retrograde pyrope rim	Phl	2		28	17					12542	118	

Table 2 SIMS trace element and H_2O data for selected minerals in whiteschist and country rocks. Concentrations in µg/g. n represents number of repeats. * denotes the mean exluding outlier data points. See text for discussion. Mineral abbreviations after Whitney and Evans (2010).

Mineral trace element and isotope compositions

Trace elements and H_2O

In the metagranite the Ti-rich phengites are enriched in B, Be and Sr compared to their parent biotites, and depleted in Li, Cs and F. Rb is very similar (Figure 5, Table 2). The Ti-poor phengites have lower Be, Rb, Cs, F, Li but higher B and Sr compared to Ti-rich phengites. K-feldspar contains large amounts of Sr and minor Rb but is otherwise not a significant host of trace elements. In the orthogneiss, phengite is rich in B, having similar contents to the Ti-poor phengite in the metagranite. Phengite is also the main host of Be and a significant host of Rb, Li and F. Biotite is the main host of Rb, Li, Cs, F and Cl, and epidote dominates the budget of Sr.

In the bulk rock, whiteschists are enriched in Mg, and depleted in Na, Ca, Fe, Sr, Rb and Li compared to the metagranite and orthogneiss (Schertl and Schreyer, 2008). Of the prograde minerals present as inclusions in Prp I, phlogopite has the highest concentrations of Li, B, Rb, Cs, Sr and F of all the minerals measured (sample DM1.1). Ellenbergerite is a significant host of Be, which correlates positively with Mg content, and a minor host of B, F and Cl. Ellenbergerite also contains large amounts of H_2O (6.0–8.8 wt%) compared to other minerals (Tlc: 3.5 wt%, Phl: 4.5–5.1 wt%). The K-deficient phlogopite present as inclusions in Prp I contains higher H_2O contents than "normal" phlogopite coexisting with Phe III (4.1 wt%). All other trace elements are present in negligible amounts. Talc hosts only Cl, and minor F and B. Kyanite is not a significant host of any of the measured trace elements. No N data were collected for these phases.

Compared to phlogopite, ellenbergerite and talc, whiteschist phengite in the matrix and as inclusions in Prp II is strongly enriched (>3x) in Li, B and

Rb, and slightly enriched (1–3x) in Be and Sr (Figure 5). F contents are lower than phlogopite but similar to talc, and Cl is much lower in phengite than any of the earlier prograde minerals. Whiteschist DM6 contains all three phengite generations and has the most complete record of their trace element evolution. Li, Be, Rb, Sr, Cs and Cl contents are similar in all phengite generations. B contents are similar in Phe II and III (172–202 µg/g) but higher in Phe I (240–292 µg/g, one outlier grain with 189 µg/g). F is high in Phe II (2047–2253 µg/g) and lower in Phe I and III (1195–2066 µg/g). N contents in Phe I range from 37–41 µg/g, whereas N contents in Phe II range from 14–53 µg/g. Phengite III has elevated N contents (64–530 µg/g, n=5) compared to other phengites. Phengite in other whiteschists contains mostly similar trace element concentrations to DM6, although B is notably higher in DM1b (342–402 µg/g), and Sr and Rb are slightly lower. Whiteschist phengite is depleted in N, Be, Li, Rb and Cs compared to metagranite phengite, and enriched in B and Sr. Whiteschist phengite has similar B contents to orthogneiss phengite, but Li, Be, Rb and Cs are lower in whiteschists, and Sr and Be are higher.

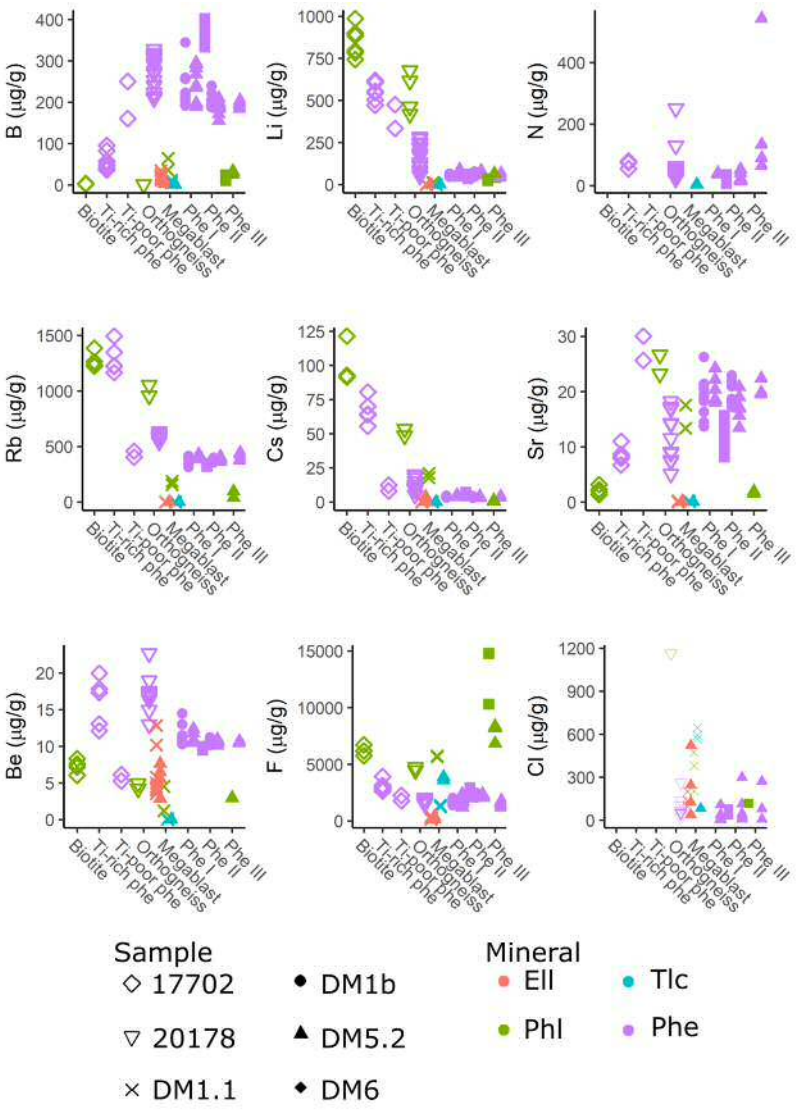

Figure 5 SIMS trace element concentrations for white micas, biotite, ellenbergerite and talc in metagranite (sample 17702), orthogneiss (sample 20178) and whiteschist (DM samples). Metagranite minerals are separated into texturally distinct categories (biotite, Ti-rich phengite, Ti-poor phengite , see 'Sample descriptions and major element compositions' section for details). Orthogneiss minerals are texturally related and so are plotted under one category. Whiteschist minerals are also separated into texturally distinct categories. Megablast consists of inclusions in pyrope megablast cores (Prp I). Phe I, II and III are different textural generations of phengite. Phe III is texturally associated with phlogopite, which is plotted under the same category in a different colour (see legend).

Boron isotopes

Boron isotope data is presented in Figure 6. In the metagranite, δ^{11}B values for Ti-rich phengite are -11.9 to -7.9 ‰ (n=5). Ti-poor phengite has lower, but overlapping values (-13.0 to -9.2, n=2). Orthogneiss has a larger range of δ^{11}B values (-15.4 to -5.7 ‰, n=8).

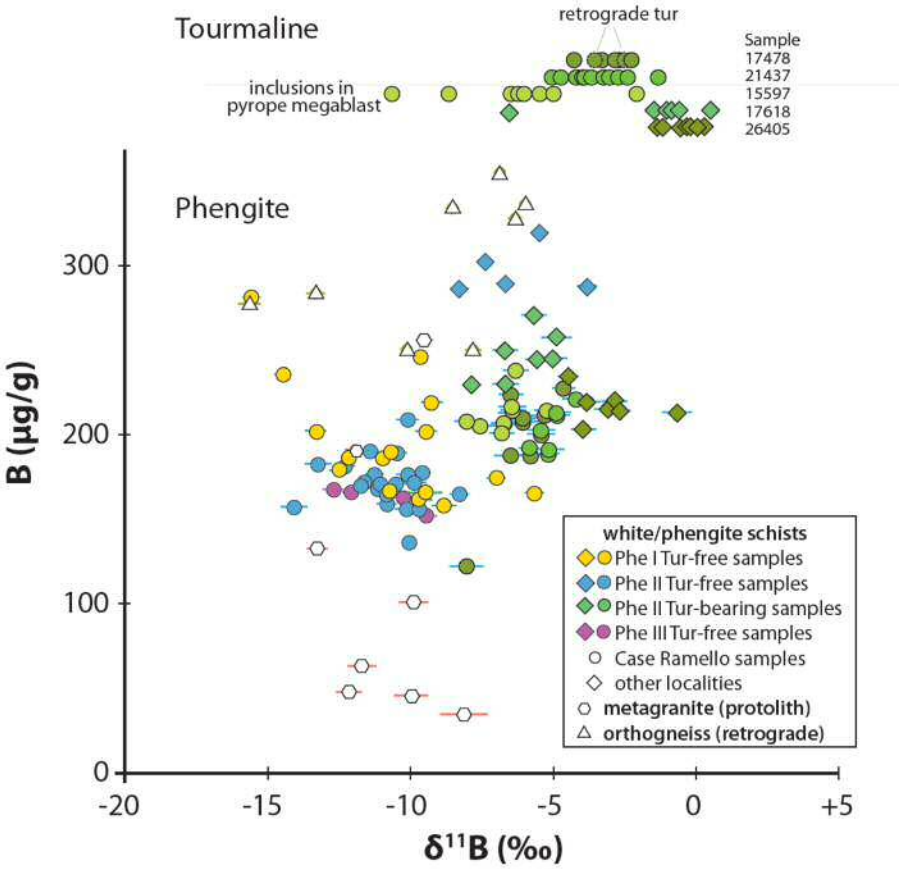

Figure 6 *Top panel:* δ^{11}B values in tourmaline from whiteschist and phengite schist. Uncertainties are smaller than symbol size. *Bottom panel:* δ^{11}B versus B concentration plot for phengite with 1s error bars. δ^{11}B is variable between different grains within the same sample but there are no strong correlations between δ^{11}B and B concentrations. Whiteschist and phengite schist divided into samples from Case Ramello (circles) and samples from other localities (diamonds). Case Ramello samples have heavier δ^{11}B and higher B contents in samples which contain tourmaline compared to those without (see text for discussion). Also shown are phengites from the metagranite and orthogneiss.

Phengite δ^{11}B in tourmaline-absent whiteschists ranges from -15.4 to -3.5 ‰ and therefore overlaps with both of the protolith lithologies. Both samples from Case Ramello have similar values (DM6 -15.3 to -8.0 ‰, DM5.2 -13.0 to -5.4 ‰), whereas the sample from Tapina has heavier values (-8.0 to -3.5 ‰). There is no significant difference between the mean δ^{11}B values of different phengite generations from the same sample, but Phe I has a wider range of δ^{11}B values than Phe II or III. There are no correlations between B concentrations and δ^{11}B of phengite in any of the samples that we analysed.

Tourmaline-bearing whiteschists and phengite schists were also analysed for B isotopes in tourmaline and phengite (Phe II). There are significant systematic differences in B concentration and isotopic composition of phengite in samples with and without tourmaline, even if both are from the same locality (Case Ramello). Here, Phe II in tourmaline-bearing samples has a mean B isotope composition of -6.0 ± 1.0 ‰ (n=26) with 198 ± 20 µg/g B. Phe II in tourmaline-absent samples has a consistently lighter B isotope composition (-10.6 ± 1.2‰, n=25) and contains less B (171 ± 14 µg/g). Phe I in these samples has a larger range of B isotope values (-10.3 ± 2.6‰, n=16) and B concentrations (196 ± 34 µg/g). Tourmaline from these samples has δ^{11}B values ranging from -10.7 to -1.4 ‰ (mean = -5.1±1.8 ‰ (n=56)). Phengite in phengite schist from other localities (samples 26405, 17618) has heavier δ^{11}B than Case Ramello for both phengite (26405 -4.5 to -0.7 ‰, 17618 -6.7 to -4.9 ‰) and tourmaline (26405: -1.8 to +0.3 ‰, 17618: -1.5 to +0.5 ‰ [one outlier -6.5 ‰]). Some tourmaline grains have a narrow rim of ca. 50–150 µm which is around 1 ‰ lighter than the core of the grain. In samples where both tourmaline and phengite are present, the difference in boron isotope composition between coexisting matrix phengite (Phe II) and tourmaline is small but somewhat variable, with mean $\Delta^{11}B_{Phe-Tur}$ of -1.6, -2.6 and -5.0 ‰ in three

separate samples. The difference between tourmaline rims and immediately adjacent phengite grains ranges from -3.7 to -1.1 ‰ (one outlier at +4.3 ‰).

Discussion

Element mobility during whiteschist prograde metamorphism: implications for fluid sources

The whiteschists underwent several major mineralogical changes during their metamorphic evolution, which are critical to understanding the fluid-mobile element evolution, and are divided into six stages (A-F; Figure 7). In this section we review the key reactions which lead to the formation of different mineral assemblages, and discuss the budget of major and trace elements associated with these reactions, to gain insight into element mobility.

Key prograde mineral reactions

Prp I (garnet megablast cores) formed by the reaction kyanite + Mg-chlorite + talc → pyrope + H_2O (Schertl et al., 1991; Ferrando et al., 2009). It is Mg-rich, and contains Mg-rich inclusions, which implies that Mg-metasomatism took place before the onset of garnet growth. The earliest prograde assemblage is preserved as inclusions in some pyrope megablast cores and consists of Mg-chlorite, kyanite, talc and rare muscovite (stage A, Figure 7). Crystallization pressure for this assemblage has been constrained to $\sim$ 1.7–2.1 GPa based on the Si content of muscovite (6.36 Si pfu Ferrando et al. (2009); Hermann (2003)). Therefore Mg-metasomatism took place during the early part of the subduction history, or prior to subduction altogether. Based on the most recent prograde P-T path published for the BIU (Groppo et al., 2019), a temperature estimate of 520–540 °C can be obtained from these pressures. Most pyrope megablasts also contain the inclusion assemblage ellenbergerite,

talc, phlogopite, kyanite and rutile (stage B). This assemblage formed on the prograde path by the reactions Mg-chlorite + kyanite + talc + rutile → ellenbergerite, and Mg-chlorite + muscovite → kyanite + phlogopite + talc + H_2O (Ferrando et al., 2009; Schertl et al., 1991). During the later prograde evolution, the reaction phlogopite + kyanite + talc → pyrope + phengite + H_2O replaces phlogopite with phengite (Schertl et al., 1991; Hermann, 2003), and grows additional Prp I (stage C). All the mentioned reactions also create fluid. Talc is found as inclusions in pyrope megablasts and small pyropes but not in the matrix so talc-out occurred later on the prograde path compared to ellenbergerite or phlogopite. Phase equilibrium modelling suggests that talc breakdown occurs gradually, over a wide P-T range, but that a final phase of fluid release occurs at ∼ 700–710 °C at >3.8 GPa (stage D), close to the metamorphic peak, by the reaction talc + kyanite → pyrope + coesite + H_2O (Gauthiez-Putallaz et al., 2016). This reaction grew Prp II (megablast rims and matrix garnet) which contains the inclusion assemblage kyanite + talc + coesite (Schertl et al., 1991; Ferrando et al., 2009; Hermann, 2003).

Element mobility during prograde reactions

The phlogopite breakdown reaction (phlogopite + kyanite + talc → pyrope + phengite + H_2O) is of particular interest in assessing the trace element mobility during prograde metamorphism, since both the products and reactants are significant hosts of fluid-mobile elements. Using the measured compositions of prograde phlogopite, phengite, pyrope and talc, and assuming pure kyanite, we calculated the stoichiometry of the phlogopite breakdown reaction by mass balancing K_2O, MgO, Al_2O_3, SiO_2 for the products and reactants. Then, using the measured H_2O contents of the products and reactants, we calculated the mass of H_2O released. The calculated stoichiometry (by mass) is 1.72 phlogopite + 0.55 talc + 0.84 kyanite → 1 phengite + 2.03 pyrope + 0.07 H_2O.

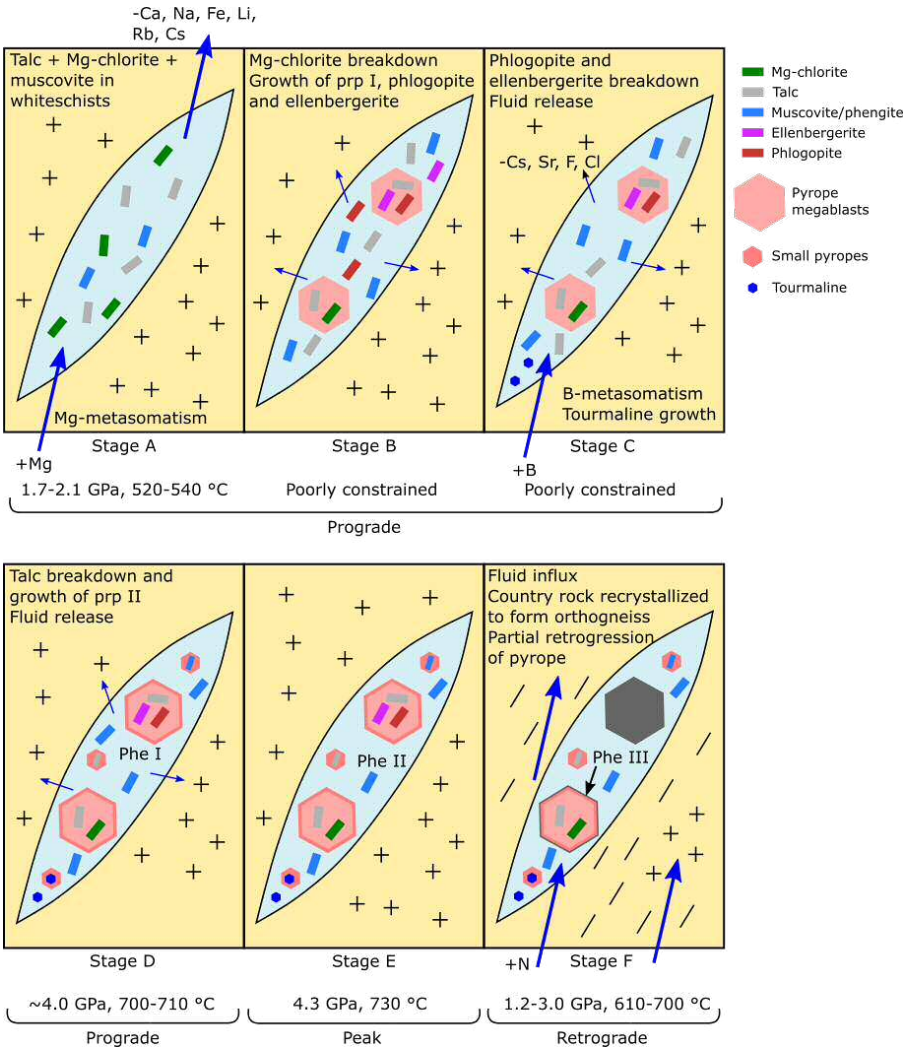

Figure 7 Metasomatic and metamorphic evolution of the whiteschists. P-T conditions for prograde stages B and C are poorly constrained because this part of the prograde path is largely constrained from other lithologies which are difficult to correlate with the whiteschist mineralogy. Large blue arrows indicate external fluid fluxes, whereas small blue arrows indicate internally derived fluids.

By volume the stoichiometry is 1.79 phlogopite + 0.58 talc + 0.68 kyanite → 1 phengite + 1.57 pyrope + 0.15 H_2O. More phlogopite is consumed than phengite is produced because the measured phlogopite composition is deficient in K_2O. In order to balance the MgO contents, this leads to a large production of pyrope. This is problematic because if all the phengite in the whiteschists

(∼ 25–50 vol%) was produced by this reaction, then the total product volume would be close to or greater than 100%. Since there are no other K-bearing phases which could break down to form phengite during prograde metamorphism, this suggests that phengite was in fact present throughout the prograde evolution, which is consistent with the thermodynamic modelling of Gauthiez-Putallaz et al. (2016). Schertl et al. (1991) found a single prograde phengite as an inclusion within a kyanite inclusion in Prp I, which is consistent with our conclusion. The reason why phengite inclusions are so rare in Prp I may relate to compositional heterogeneity in the whiteschist (Hermann, 2003). Phlogopite formed via reaction of Mg-chlorite and muscovite and therefore, in chlorite-rich domains, muscovite could be largely consumed during the formation of phlogopite. Since the first pyrope-forming reaction also involves Mg-chlorite as a reactant, these Mg-chlorite-rich domains also likely gave rise to the pyrope megablasts, which preserve the prograde inclusion assemblages. Prograde phengite would have been stable in the chlorite-poor matrix (see Figure 7) but it re-equilibrated at peak conditions and is not preserved. This is consistent with the experimental phase equilibria of Hermann (2003), which show that phengite is stable under SiO_2-saturated conditions (matrix), whereas phlogopite is stable under SiO_2-undersaturated conditions (megablasts).

Of the reactant phases in the phlogopite breakdown reaction, kyanite is not a significant host of any trace elements that we measured, talc contains only F and minor B, and phlogopite is a significant host for multiple trace elements. Of the product phases, phengite hosts multiple trace elements, whilst garnet only contains significant amounts of Li. Compared to the later forming phengite, phlogopite contains less Li, B, Be and Rb, slightly less Sr, and substantially higher Cs and F. Ellenbergerite is also a significant host of B and Be. Using the reaction stoichiometry calculated for phlogopite breakdown and

the phlogopite and talc trace element compositions measured from DM1.1, the trace element budget of the reactants can be calculated (Table 3). Comparing this budget to the measured compositions of Phe I and Prp II, there is not enough Li, B, Be and Rb in the phlogopite + talc assemblage to account for the measured phengite composition, if all of the trace elements in the products were sourced from phlogopite breakdown (i.e. there was no phengite/pyrope coexisting with phlogopite). For Sr, there is a slight excess in the reactant minerals compared to the products, and for Cs, F and Cl there are large excesses. The contribution of ellenbergerite cannot be assessed quantitatively using this method because the reaction through which it breaks down is not known, and likely does not involve phengite. However, the concentration of all these trace elements, except Cl, is lower in ellenbergerite than in phengite (by at least an order of magnitude for all elements except Be) so it would require large modal abundances of ellenbergerite relative to phengite in order to make up the missing concentrations of Li, Be, B and Rb. By comparing the measured Zr, P and Ti contents of ellenbergerite to average bulk contents reported in Schertl and Schreyer (2008), we calculate that the ellenbergerite mode is unlikely to have exceeded 5% (Online Resource 3), and cannot therefore account for the missing trace elements. These missing concentrations suggest that either there was addition of these elements to the whiteschist during prograde metamorphism, or there is a missing reservoir of these elements which we have not measured. This missing reservoir could be prograde phengite, as there are not any other obvious candidate minerals which are rich in Li, B, Be and Rb. This matches our earlier conclusion from the major element mass balance of phlogopite breakdown. Alternatively, or perhaps additionally, external fluids rich in B, Li, Rb and Be infiltrated the whiteschist during prograde metamorphism and resulted in addition of these elements around stage C (Figure 7).

	Mineral	Li	B	Be	Rb	Sr	Cs	F	Cl
Avg. conc. (µg/g)	Ell	0.32	17	6.0	0.02	0.08	0.50	246	153
Avg. conc. (µg/g)	Tlc	0.59	5.7	0.05	0.07	0.12	<0.01	2076	471
Avg. conc. (µg/g)	Phl	11	50	2.9	172	15	19	5695	352
Avg. conc. (µg/g)	Phe I	58	237	11	395	20	3.9	1645	42
Avg. conc. (µg/g)	Prp II	22	<0.01					34	
	Stoichiometry	**Li**	**B**	**Be**	**Rb**	**Sr**	**Cs**	**F**	**Cl**
Phl budget (µg/g)	1.72	19	86	4.9	296	27	33	9821	607
Tlc budget (µg/g)	0.55	0.09	4.4	0.04	0.06	0.08	<0.01	729	333
Phe budget (µg/g)	1	58	237	11	395	20	3.9	1645	42
Prp budget (µg/g)	2.03	22	<0.01					69	
Reactants/products		24%	38%	44%	75%	137%	851%	616%	2215%

Table 3 Top panel: trace element concentrations in reactant and product phases involved in the phlogopite breakdown reaction. Ellenbergerite is also shown for comparison since it breaks down at similar conditions to phlogopite. Bottom panel: trace element budgets of the reactant and product phases involved in phlogopite breakdown. See text for calculation details and interpretation (Element mobility during whiteschist prograde metamorphism, and its implications for fluid sources).

Whiteschist phengites are significantly enriched in B compared to those in the metagranite ($\sim$ 4x enrichment) and coupled with the higher phengite mode in whiteschist, this leads to 10–20x bulk enrichment of B in the whiteschist compared to metagranite, supporting the conclusion that a substantial amount of B was added to the whiteschist during metasomatism.

For Cs, Sr, F and Cl, the excess of these elements in the reactants of phlogopite breakdown compared to the solid products suggests that these elements were liberated into prograde fluids and lost from the bulk rock. High Cl contents in phlogopite (203–474 µg/g), ellenbergerite (41–522 µg/g) and talc (565–645 µg/g) compared to the measured phengite (5.3–299 µg/g, mean=43 µg/g, excluding 3 outliers with Cl> µg/g) are consistent with the presence of brines during early prograde metasomatism, and the subsequent evolution of the fluid-phase towards a Cl-poor fluid (Ferrando et al., 2009). Phengite-fluid ($D_{Cl}^{Phe-Fl} = 0.001$) and biotite-fluid ($D_{Cl}^{Bt-Fl} = 0.008$) partition coefficients for Cl in UHP eclogites can be calculated from the data in Svensen et al. (2001). Using these values, the Cl content in the fluid coexisting with

prograde phlogopite is estimated at 2.5–6 wt%. This is comparable to the values of 3.6–17 wt% calculated by Ferrando et al. (2009) from microthermometry of fluid inclusions in prograde kyanite.

The trace element data therefore suggest that the external fluid composition evolved from Cl-rich during early prograde metamorphism (stage B) to Cl-poor and B, Be, Rb, Li-rich later on the prograde path (stage C). Most previous studies considered only a single major external fluid influx event (Mg metasomatism) followed by predominantly internally-derived fluids (e.g. Chen et al., 2016; Schertl and Schreyer, 2008; Sharp et al., 1993; Tian et al., 2019; Chen et al., 2019; Xiong et al., 2022; Ferrando et al., 2009; Gauthiez-Putallaz et al., 2016; Chen et al., 2023). We suggest that later B, Be, Rb, Li-rich fluids were derived from a distinct external source. This is supported by the composition of the orthogneiss: B contents are much higher in orthogneiss phengite than in Ti-rich phengite in metagranite by about a factor of 3. There are no additional B-rich phases in the metagranite which could break down to release B during recrystallization so this suggests that B was added to the orthogneiss during its metamorphic history. Thus, the orthogneiss has experienced B-metasomatism but not Mg-metasomatism. The occurrence of two separate metasomatic event in the whiteschists raises the possibility that different external fluid sources may explain different aspects of the whiteschist geochemistry (e.g. later B-rich vs earlier Mg, Cl-rich fluids), especially if the later event only partially overprinted the first event.

Effects of retrograde fluid addition

In the whiteschists, the retrograde stage is represented by Phe III, which occurs as fibrous phengite + phlogopite coronae on pyrope rims (stage F). These record the reaction pyrope + phengite + H_2O → phlogopite + kyanite +

talc, which occurred during retrogression at ∼ 2.5–3.0 GPa, 670–700 °C (Hermann, 2003). This reaction requires fluid input so Phe III and the associated phlogopite record the composition of retrograde fluids interacting with the whiteschist. There is little difference in B concentrations between Phe II and Phe III. Phe III has highly variable N contents (64–543 µg/g) but all grains are enriched in N compared to other phengite generations (14–41 µg/g), suggesting that N was added during retrogression. Two points measured on the rims of Phe II grains also have elevated N compared to other Phe II analyses and therefore seem to record the same retrograde signal as Phe III. The strong N enrichment in Phe III suggests an interaction with sediment-derived fluids, since sediments are the only common lithology which contains high N contents (100s–1000s µg/g, Johnson and Goldblatt (2015) and references therein). Phe III contains less F than Phe II, and slightly less Li, but other trace elements are similar. Coexisting phlogopite has slightly higher Li contents than Phe III (65 µg/g vs. 42–61 µg/g), but contains much lower concentrations of all other trace elements, except F. The Li and F depletion in Phe III compared to Phe II may therefore be due to incorporation of Li and F into phlogopite.

Boron isotope constraints on metasomatic fluid compositions

Apart from some rare tourmaline-bearing samples, phengite is the major host for B in the metagranite and whiteschists and records information about B contents and isotopic composition of the metasomatic fluid. We will first discuss the record that phengite provides of the metasomatic fluid composition, and then compare this to the record in tourmaline.

At the conditions of B metasomatism (∼ 600–700 °C), the B isotope fractionation between phengite and fluid is $\Delta^{11}B_{Phe-Fluid}$ = -11.2 to -9.3 ‰, for

fluids that are neutral to acidic (Kowalski et al., 2013). Acidic fluids have been assumed in previous B isotope studies in order to explain the marked decrease in B isotope composition of the subducted slab with increasing depth (e.g. Konrad-Schmolke et al., 2016; Peacock and Hervig, 1999). Recent modelling work has suggested that fluids in equilibrium with crustal lithologies at subduction zone conditions should be moderately alkaline (pH 1.5–3 units above neutrality Galvez et al. (2016)) and this would result in a much smaller phengite-fluid B isotope fractionation (-3.2 to -2.6 ‰ at 600–700 °C, Kowalski et al. (2013)). However, tourmaline is only stable in acidic fluids (Morgan and London, 1989; Marschall et al., 2006) so the growth of tourmaline in our samples suggests that the fluids were in fact acidic. Whiteschist phengite B isotope compositions range from -15.6 to -3.8 ‰ (mean = -10.1 ± 2.3 ‰), suggesting a fluid composition between ∼ -6 and +7 ‰, assuming high fluid-rock ratios that completely overprinted the B isotope signature of the protolith (δ^{11}B = -8 to -13 ‰), or somewhat higher δ^{11}B if fluid-rock ratios were low. In any case, independent of the composition of the fluid, and as long as temperature is comparable, the source lithology of the fluid will have had a δ^{11}B value comparable to phengite in our samples (ca. -10 ‰), as in most subducting lithologies, B will be hosted in minerals with similar B coordination as phengite, which is what controls B fractionation. There is some heterogeneity in phengite B isotope compositions within samples and particularly between different localities, suggesting that the fluid composition may have been variable or multiple episodes of fluids of different compositions were recorded. Phengite B contents in whiteschist range from 155–344 µg/g. Reported phengite-fluid partition coefficients for B in HP rocks range from 0.2–0.7 (Marschall et al., 2006; Brenan et al., 1998; Adam et al., 2014), which suggests that B concentrations in the metasomatic fluid were in the range of 220–1720 µg/g, assuming

element concentrations in phengite were not affected by changes in mineral modal abundance subsequent to fluid-rock interaction. As K_2O appears to have behaved conservatively during metasomatism (Schertl and Schreyer, 2008) and phlogopite, the only other K-bearing phase, was only stable during a short section of the prograde path, we conclude B in phengite reflects equilibrium with the B-rich fluid. This is supported by limited variation of B in different phengite generations and between samples. Thus, the B-rich fluid contained ca. 500 µg/g with a δ^{11}B of 0 ± 6 ‰.

Previously proposed sources for an Alpine metasomatic fluid include slab serpentinite (Sharp and Barnes, 2004; Ferrando et al., 2009), mantle wedge serpentinite (Chen et al., 2016; Tian et al., 2019) and altered oceanic crust (AOC) (Sharp et al., 1993; Demény et al., 1997). Fresh MORB contains 1.2 µg/g B and depleted mantle contains 0.08 µg/g B so these cannot be sources of B-rich fluids during subduction (Marschall et al., 2017). AOC has variable B isotope values from -4 ‰ to +25 ‰, with an average of +3.4 ‰ (Smith et al., 1995), and B contents of up to 100 µg/g, but averaging to values <10 µg/g since the B content depends strongly on the degree of alteration (Smith et al., 1995; Yamaoka et al., 2012; Marschall, 2018). AOC itself is therefore unlikely to be a source of B-rich, isotopically light fluids. Lighter isotope signatures can be generated by slab dehydration during subduction (Marschall et al., 2007) but this also depletes B, so deep AOC-derived fluids which are both B-rich and isotopically light are therefore highly unlikely. Slab-hosted serpentinites have δ^{11}B $> +10$ ‰ (De Hoog and Savov, 2018; Martin et al., 2020; Clarke et al., 2020), so our isotopic composition for the metasomatic fluid is not consistent with a pure slab serpentinite source.

Mantle wedge serpentinites form by hydration of the dry mantle wedge by fluids derived from the subducting slab. Shallow (forearc) mantle wedge

serpentinites can have high B contents (up to 80 µg/g) and heavy B isotope compositions (+15 to +25 ‰) (De Hoog and Savov (2018) and references therein), whereas deep mantle wedge serpentinites have a range of B isotope values from +3 ‰ down to around -14 ‰, averaging to ca. -5 ‰ (De Hoog and Savov, 2018; Martin et al., 2020). The latter would be consistent with our suggested isotopic composition of the metasomatic fluid. However, these deep antigorite serpentinites contain <60 µg/g B, averaging to ca. 20 µg/g (De Hoog and Savov, 2018; Martin et al., 2020; Yamada et al., 2019). Major fluid release from serpentinites occurs mainly during antigorite breakdown at ca. 650°C. The amount of fluid released is 6–13 wt%, depending on the serpentinite composition (Padrón-Navarta et al., 2013; Ulmer and Trommsdorff, 1995), with B contents in the fluid (150–330 µg/g, based on 20 µg/g bulk B and 6-13 wt% fluid release) in the lower end of the range calculated for the metasomatic fluid (220-1720 µg/g, see above). However, up to 30 µg/g B can be retained in metamorphic olivine formed during antigorite breakdown (Clarke et al., 2020; De Hoog et al., 2014), which would reduce the amount of B released in the fluid. Fluid transport modelling suggests that B contents in fluids released from mantle wedge serpentinites could reach up to ca. 200 µg/g (Konrad-Schmolke et al., 2016), similar to our simple estimate, although fluid inclusions in HP antigorite serpentinites measured by Scambelluri et al. (2004) had lower B contents (1–50 µg/g, but mostly <20 µg/g, for bulk rock B contents ∼10 µg/g). Overall, fluids generated purely from dehydration of mantle wedge serpentinite are unlikely to explain the high B contents in the metasomatic fluid as recorded by phengite. Earlier fluids that caused Mg metasomatism likely contained B, and these may indeed have been derived from serpentine dehydration, but the majority of B in the rocks appears to be have been derived from other sources.

The B isotope composition of the Mg-rich fluids is not preserved in phengite, since it was overprinted by the later B-rich fluids.

Sediments are another potential source of B-bearing fluids in subduction zones. Carbonate sediments have very heavy B isotope compositions (>20 ‰), but other oceanic sediments (e.g. pelagic clays, siliceous ooze, turbidites) can have negative B isotope values down to -13 ‰, with most values falling between -10 to 0 ‰ (Tonarini et al., 2011; Ishikawa and Nakamura, 1993; Marschall, 2018). Boron contents are mostly in the range 50–150 µg/g. Fluids sourced from subducted sediments are consistent with the negative B isotope values of whiteschist phengite and and can also explain the high B contents calculated for the metasomatic fluid. White mica hosts >80% of the B in most meta-sedimentary rocks (Bebout et al., 2007; Marschall et al., 2006). The average K_2O content of subducted sediments (excluding carbonates) is $\sim$ 2.5 wt% (Plank, 2014), which results in $\sim$ 25% white mica mode in the meta-sediment. Therefore whole rock B concentrations of 50–150 µg/g translate to white mica B concentrations of 120–360 µg/g, which is similar to the range in whiteschist phengite, and therefore whiteschists could be in equilibrium with a sediment-derived fluid.

Comparison with previous evidence for fluid compositions

Whiteschist trace elements do not present a clear argument in favour of either serpentinite or sediment-derived fluids. There is no enrichment in Ni and Cr in the whiteschists compared to their protoliths (Schertl and Schreyer, 2008). These elements are commonly enriched in serpentinite-derived fluids (e.g. Angiboust et al., 2014; Penniston-Dorland et al., 2010), including in mantle-wedge serpentinites (Martin et al., 2020), and the lack of enrichments in these were used to argue against serpentinite-derived fluids in the metasomatism of Monte

Rosa whiteschists (Luisier et al., 2021). On the other hand, the whiteschists are depleted in many large ion lithophile elements (Na, Rb, Ba, Sr) compared to their protoliths, and these elements are commonly enriched in sediment-derived fluids (e.g. Sorensen et al., 1997; Sievers et al., 2017). K is a major exception to this, behaving rather conservatively in the whiteschists despite its high solubility in HP fluids (Connolly and Galvez, 2018), which suggests metasomatic fluids were probably K-rich, or else K would have been leached from the rocks (Luisier et al., 2021).

Previous studies discounted sediments as a source for the metasomatic fluid on two main grounds. The whiteschists have light oxygen isotopes (whole rock δ^{18}O=7.4–8.4 ‰, Gauthiez-Putallaz et al. (2016), Sharp et al. (1993), Chen et al. (2016)), which are much lower than values for sediments. Additionally, fluids derived from sediment dehydration have low Mg contents (Herviou et al., 2021; Manning, 2004), which does not explain the Mg enrichment in whiteschists. Magnesium isotope data are also consistent with a talc-bearing serpentinite source for the fluid (Chen et al., 2016). Due to the high oxygen concentrations of rocks, resetting of whole rock O isotope signatures requires large fluid-rock ratios. If the amount of B-rich fluid was small compared to the earlier Mg-metasomatism then O isotopes would likely still reflect the Mg-rich fluid source. *In situ* O isotopes have been measured in garnet, zircon, quartz, kyanite and phengite (Sharp et al., 1993; Gauthiez-Putallaz et al., 2016; Chen et al., 2017). The extent of zircon O isotope resetting during fluid-rock interaction is known to be variable (Rubatto, 2017). Other anhydrous minerals (garnet, quartz, kyanite) may also be expected to respond slowly to fluid-rock interaction. For phengite, there was a difference between the measured O isotope composition and the value predicted by closed-system fractionation, which was attributed to issues with fractionation factors and inter-sample

comparison (Gauthiez-Putallaz et al., 2016), but could alternatively reflect a partial resetting of hydrous mineral O isotopes by B-rich fluids. As B metasomatism was separate from Mg metasomatism, neither the Mg-rich nature of the whiteschists, nor the Mg isotope data present a difficulty for our model, as Mg is a structural component of the main rock-forming minerals in whiteschists, and therefore requires large fluid-rock ratios to reset. In contrast, Li is a much more fluid-mobile element and is therefore likely to have been affected by fluid influx during B metasomatism. This may explain the lack of correlation between bulk Li concentrations, Li isotopes, and other isotope systems, as reported by Tian et al. (2019). Furthermore, significant kinetic isotope fractionation of Li can occur during garnet growth at HP conditions (Bebout et al., 2022). This could be significant in the whiteschists due to the large modal abundance of garnet, and adds to the complexity of interpreting the Li isotope data. Finally, recently published Ba isotope data (Chen et al., 2023) are consistent with either a sediment-derived fluid or a mantle wedge serpentinite-derived fluid, since the Ba isotope signature of mantle wedge serpentinites is inherited from the slab-derived crustal fluids that formed them. Thus, a two stage model where the second stage involves a dominantly sediment-derived fluid is consistent with our own as well as previous isotope data.

Although the majority of B appears to have been sourced from sediments, it is possible that the B metasomatic fluid also contained a serpentinite-derived component, but this would have contributed little B due to the lower concentration of B in serpentinites. Several studies of serpentinite dehydration have observed open system behaviour, where dehydrating serpentinite is fluxed by B-rich, isotopically light, sediment derived fluids (Clarke et al., 2020; Harvey et al., 2014). The sediment-derived component can comprise at least 15-45% of the total fluid budget leaving the serpentinite, and the resulting fluid would

conceivably have mixed characteristics in terms of B contents and isotopes as well as other elements. This represents an alternative scenario of generating a mixture of sediment and serpentinite-derived geochemical signatures in the whiteschist. It would be difficult to distinguish such fluids from fluids derived from mantle-wedge serpentinites, which themselves formed by metasomatism of mantle peridotite by slab-derived crustal fluids.

Finally, it is worth noting that the whiteschists and associated metasomatic rocks constitute a volumetrically minor part of the entire Brossasco-Isasca UHP Unit. External fluids which affected the whiteschists therefore must have traversed a significant portion of the rest of the unit to reach the whiteschists, including metasediments. So it is possible that the sedimentary B isotope signature of the metasomatic fluids was acquired locally during transport and that the original source of the fluids has been obscured. Nevertheless, this would not explain Mg metasomatism, so does not affect our interpretation that these were distinct fluid infiltration events.

The differing records of tourmaline and phengite B isotopes

Rare tourmaline-bearing samples (<1% of all samples) of metagranite, orthogneiss, whiteschist and phengite schist provide an additional window into B behaviour during metasomatism. Our own B isotope data for tourmaline in these rocks matches data presented by Xiong et al. (2022). They explained the compositions of metasomatic whiteschist tourmaline by reaction of isotopically light tourmaline in the metagranite (-13.3 to -5.5 ‰) with isotopically heavier fluid (>+2.4 ‰: the fluid in equilibrium with the heaviest measured tourmaline) derived from dehydration of mantle wedge serpentinite (Mg metasomatism). If tourmaline grew during Mg metasomatism, then its B isotope

composition should be unrelated to that of phengite, which we have argued was acquired during later B-metasomatism. Figure 8 shows the B isotope composition of a hypothetical phengite in equilibrium with tourmaline at prograde to peak conditions. This overlaps with the range of phengite B isotope compositions observed in tourmaline-absent samples, suggesting that tourmaline and phengite could therefore have equilibrated with the same B-rich fluid during B-metasomatism. High B concentrations in the fluid would explain the crystallization of tourmaline at this stage (stage C, Figure 7). This timing of tourmaline growth is supported by the observation than most tourmaline occurs in the matrix or as inclusions in prp II. Tourmaline inclusions in prp I are very rare (none were observed in this study but they were documented in at least one sample by Schertl et al. (1991)). Inclusions in prp I may reflect igneous tourmaline from the protolith that was recrystallized during Mg-metasomatism as suggested by Xiong et al. (2022) for sample 15597. The large variation of tourmaline B isotope values in this sample reflects incomplete re-equilibration with external fluid, whereas the relatively small range of tourmaline B isotope compositions in other samples suggest complete (re-)crystallization with a fluid, likely during B metasomatism.

In samples where both tourmaline and phengite are present, the boron isotope fractionation between coexisting matrix phengite (Phe II) differs significantly from predicted equilibrium fractionation between tourmaline and mica (observed $\Delta^{11}B_{Phe-Tur}$ = -1.6 to -5.0 ‰, predicted $\Delta^{11}B_{Phe-Tur}$ = -12.3 ‰ at 530 °C (early prograde conditions) and -8.2 ‰ at 730 °C (peak conditions), Figure 8, Klemme et al. (2011); Kowalski et al. (2013); Wunder et al. (2005)). Furthermore, Phe II in tourmaline-bearing samples contains more B and has a heavier B isotope composition than Phe II in tourmaline-absent samples from the same locality (Case Ramello). Phe II in tourmaline-bearing samples

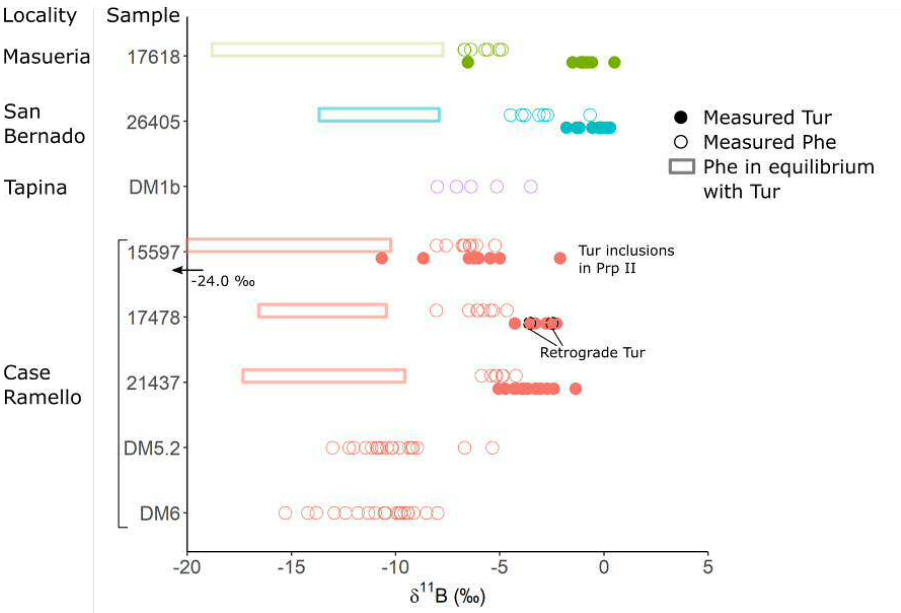

Figure 8 δ^{11}B values in tourmaline and phengite from whiteschist and phengite schist. 1s uncertainties for tourmaline are smaller than symbol size. Also shown is the range of δ^{11}B values which would represent phengite in isotopic equilibrium with tourmaline (see text for discussion). Phengite and tourmaline are therefore not in isotopic equilibrium in samples where both are present. Where tourmaline-bearing and tourmaline-absent samples are available for the same locality (Case Ramello), phengite in tourmaline-bearing samples has heavier δ^{11}B and higher B contents than in tourmaline absent samples (see text for discussion).

could have interacted with a separate, isotopically heavier fluid to Phe II in tourmaline-absent samples, and to tourmaline itself. Tourmaline was not affected by this fluid due to a kinetic control, as B diffusion in tourmaline is slow as it is a structural component. Thus, isotopic disequilibrium could be preserved. As B isotope fractionation is strongly pH dependent, a change in fluid pH from tourmaline to phengite crystallisation may also have played a role. Alternatively, the fact that the anomalous B isotope composition of phengite only occurs in samples which contain tourmaline, which is a B-rich mineral, suggests that tourmaline may be involved in generating the anomalous composition. This would require some process to occur after B metasomatism which

drove the phengite and tourmaline B isotope compositions away from equilibrium, and could explain the presence of thin rims on some tourmaline grains which have a B isotope composition ca. 1 ‰ lighter than the rest of the grain.

It is unclear which of these scenarios best explains the anomalous composition of phengite in tourmaline-bearing samples, but our data indicates that caution should be applied interpreting phengite from tourmaline-bearing samples as representing equilibrium B isotope fractionation. It is important to note that tourmaline occurs only very rarely in whiteschists (<1% of whiteschists and other related metasomatic rocks contain tourmaline), and that phengite from tourmaline-absent samples dominates the whiteschist B budget at the outcrop scale. Therefore, our interpretation of the fluid sources recorded by B isotopes are unaffected by these anomalous tourmaline-bearing phengites.

Wider implications

The occurrence of whiteschists and similar Mg-rich rocks hosted within metagranitoids has been documented in multiple locations across the Alps (Ferrando (2012) and references therein). They occur in units that reached a range of peak P-T condition from greenschist facies right up to UHP eclogite facies. Our study shows that the Dora-Maira whiteschists record multiple periods of fluid influx, which occurred over a range of P-T conditions experienced during subduction, suggesting that they may represent a long-lived fluid pathway. Such pathways may transport multiple generations of fluids, not just those which led to their initial formation, and thus subduction-zone related rocks likely exhibit polymetasomatism. This may help to explain the conflicting interpretations put forward for the formation of different whiteschist bodies (e.g. Dora-Maira (our work and references herein) versus Monte Rosa (e.g. Marger et al., 2019; Pawlig and Baumgartner, 2001)).

Conclusions

Dora Maira whiteschist are strongly enriched in Mg and B compared to their granite protolith. Multiple lines of evidence point to the conclusion that the majority of B was added to the whiteschist at a later stage to the Mg-metasomatism, which produced the unusual major element composition. Firstly, mass balance analysis of the metamorphic reactions which occurred during prograde metamorphism allows us to trace the gain or loss of different elements. Our calculations suggest that there is an excess of B, Li, Rb and Be in the phases present during peak metamorphism compared to prograde phases and therefore that these elements were added by external fluids during prograde metamorphism. Secondly, high B concentrations and light δ^{11}B values in whiteschist phengite point to sediments as the main source of B-rich fluids. In some samples, tourmaline also grew during this stage and recorded B isotope compositions in equilibrium with the same fluid. Whiteschist phengite is more useful than tourmaline for recording the B concentration in the metasomatic fluid, since B behaves as a trace element in micas, and fluid compositions can therefore be directly calculated using partitioning data. Finally, the protolith orthogneiss records similarly high B concentrations in phengite but has not undergone Mg metasomatism, which further supports the separation of B and Mg metasomatic events. These conclusions fit with the previously proposed idea that fluid evolved from Mg-Cl brines to Cl-poor, aluminosilicate-rich fluids during prograde metamorphism (Ferrando et al., 2009), and they further constrain the trace element contents of these fluids. The B data imply that multiple external fluid inputs were present throughout prograde metamorphism, suggesting that the whiteschists may record a long-lived fluid pathway. This study demonstrates the utility of *in situ* analyses in unravelling complex fluid-rock interaction histories, where whole rock analyses make it difficult to

distinguish between different stages of fluid-rock interaction. Polymetasomatism of subduction-related rocks may result in decoupling of isotopic signatures for different elements.

Statements and Declarations

The authors declare that they have no known competing financial interests or personal relationships that could have appeared to influence the work reported in this paper.

Acknowledgements

We thank C. Hayward for help with EPMA analyses. This work was supported by a UK Natural Environment Research Council Doctoral Training Partnership grant (NE/ S007407/1) and UK Natural Environment Research Council Ion Microprobe Facility grants IMF 699/1119 and IMF 740/0522. Comments by three anonymous reviewers and editor Daniella Rubatto greatly improved the manuscript.

References

Adam, J., M. Locmelis, J.C. Afonso, T. Rushmer, and M.L. Fiorentini. 2014. The capacity of hydrous fluids to transport and fractionate incompatible elements and metals within the Earth's mantle. *Geochemistry, Geophysics, Geosystems 15*(6): 2241–2253. https://doi.org/https://doi.org/10.1002/2013GC005199 .

Angiboust, S., T. Pettke, J.C.M. De Hoog, B. Caron, and O. Oncken. 2014. Channelized Fluid Flow and Eclogite-facies Metasomatism along the Subduction Shear Zone. *Journal of Petrology 55*(5): 883–916. https://doi.org/

10.1093/petrology/egu010 .

Bebout, G.E., A.E. Bebout, and C.M. Graham. 2007. Cycling of B, Li, and LILE (K, Cs, Rb, Ba, Sr) into subduction zones: SIMS evidence from micas in high-P/T metasedimentary rocks. *Chemical Geology 239*(3): 284–304. https://doi.org/10.1016/j.chemgeo.2006.10.016 .

Bebout, G.E., T. Ota, T. Kunihiro, W.D. Carlson, and E. Nakamura. 2022. Lithium in garnet as a tracer of subduction zone metamorphic reactions: The record in ultrahigh-pressure metapelites at Lago di Cignana, Italy. *Geosphere 18*(3): 1020–1029. https://doi.org/10.1130/GES02473.1 .

Biino, G. and R. Compagnoni. 1992. Very-high pressure metamorphism of the Brossasco coronite metagranite, southern Dora Maira Massif, Western Alps. *Schweiz. Mineral. Petrogr. Mitt.* 72: 347–363 .

Brenan, J.M., F.J. Ryerson, and H.F. Shaw. 1998. The role of aqueous fluids in the slab-to-mantle transfer of boron, beryllium, and lithium during subduction: experiments and models. *Geochimica et Cosmochimica Acta 62*(19): 3337–3347. https://doi.org/10.1016/S0016-7037(98)00224-5 .

Bruno, M., R. Compagnoni, and M. Rubbo. 2001. The ultra-high pressure coronitic and pseudomorphous reactions in a metagranodiorite from the Brossasco-Isasca Unit, Dora-Maira Massif, western Italian Alps: a petrographic study and equilibrium thermodynamic modelling. *Journal of Metamorphic Geology 19*(1): 33–43. https://doi.org/10.1046/j.1525-1314.2001.00291.x .

Busigny, V., P. Cartigny, P. Philippot, M. Ader, and M. Javoy. 2003. Massive recycling of nitrogen and other fluid-mobile elements (K, Rb, Cs, H) in a cold slab environment: evidence from HP to UHP oceanic metasediments of the

Schistes Lustrés nappe (western Alps, Europe). *Earth and Planetary Science Letters 215*(1): 27–42. https://doi.org/10.1016/S0012-821X(03)00453-9 .

Castelli, D., F. Rolfo, C. Groppo, and R. Compagnoni. 2007. Impure marbles from the UHP Brossasco-Isasca Unit (Dora-Maira Massif, western Alps): evidence for Alpine equilibration in the diamond stability field and evaluation of the X(CO2) fluid evolution. *Journal of Metamorphic Geology 25*(6): 587–603. https://doi.org/10.1111/j.1525-1314.2007.00716.x .

Chen, A., Y.X. Chen, X. Gu, Z. Zeng, Z. Xiao, H.P. Schertl, X. Han, Z.F. Zhao, and F. Huang. 2023. Barium isotope behavior during interaction between serpentinite-derived fluids and metamorphic rocks in the continental subduction zone. *Geochimica et Cosmochimica Acta* 353: 61–75. https://doi.org/10.1016/j.gca.2023.05.016 .

Chen, Y.X., W. Lu, Y. He, H.P. Schertl, Y.F. Zheng, J.W. Xiong, and K. Zhou. 2019. Tracking Fe mobility and Fe speciation in subduction zone fluids at the slab-mantle interface in a subduction channel: A tale of whiteschist from the Western Alps. *Geochimica et Cosmochimica Acta* 267: 1–16. https://doi.org/10.1016/j.gca.2019.09.020 .

Chen, Y.X., H.P. Schertl, Y.F. Zheng, F. Huang, K. Zhou, and Y.Z. Gong. 2016. Mg–O isotopes trace the origin of Mg-rich fluids in the deeply subducted continental crust of Western Alps. *Earth and Planetary Science Letters* 456: 157–167. https://doi.org/10.1016/j.epsl.2016.09.010 .

Chen, Y.X., K. Zhou, Y.F. Zheng, and H.P. Schertl. 2017. Zircon geochemical constraints on the protolith nature and metasomatic process of the Mg-rich whiteschist from the Western Alps. *Chemical Geology* 467: 177–195. https://doi.org/10.1016/j.chemgeo.2017.08.013 .

Chopin, C. 1984. Coesite and pure pyrope in high-grade blueschists of the Western Alps: a first record and some consequences. *Contributions to Mineralogy and Petrology 86*(2): 107–118. https://doi.org/10.1007/BF00381838 .

Chopin, C., R. Klaska, O. Medenbach, and D. Dron. 1986. Ellenbergerite, a new high-pressure Mg-Al-(Ti,Zr)-silicate with a novel structure based on face-sharing octahedra. *Contributions to Mineralogy and Petrology 92*(3): 316–321. https://doi.org/10.1007/BF00572160 .

Clarke, E., J.C.M. De Hoog, L. Kirstein, J. Harvey, and B. Debret. 2020. Metamorphic olivine records external fluid infiltration during serpentinite dehydration. *Geochemical Perspectives Letters* 16: 25–29. https://doi.org/10.7185/geochemlet.2039 .

Codeço, M.S., P. Weis, R.B. Trumbull, J. Glodny, M. Wiedenbeck, and R.L. Romer. 2019. Boron Isotope Muscovite-Tourmaline Geothermometry Indicates Fluid Cooling During Magmatic-Hydrothermal W-Sn Ore Formation. *Economic Geology 114*(1): 153–163. https://doi.org/10.5382/econgeo.2019.4625 .

Compagnoni, R. and T. Hirajima. 2001. Superzoned garnets in the coesite-bearing Brossasco-Isasca Unit, Dora-Maira massif, Western Alps, and the origin of the whiteschists. *Lithos 57*(4): 219–236. https://doi.org/10.1016/S0024-4937(01)00041-X .

Compagnoni, R., B. Messiga, and D. Castelli 1994. High pressure metamorphism in the Western Alps. Guide-book to the field excursion of the 16th meeting of the IMA, September 10–15, 2004, Pisa, 148 p.

Compagnoni, R. and F. Rolfo. 2003. UHPM units in the Western Alps, In *Ultrahigh Pressure Metamorphism*, eds. Papp, G., T.G. Weiszburg, D.A. Carswell, R. Compagnoni, and F. Rolfo, 13–49. Budapest: Mineralogical Society of Great Britain and Ireland. https://doi.org/10.1180/EMU-notes.5.2.

Connolly, J.A.D. and M.E. Galvez. 2018. Electrolytic fluid speciation by Gibbs energy minimization and implications for subduction zone mass transfer. *Earth and Planetary Science Letters* 501: 90–102. https://doi.org/10.1016/j.epsl.2018.08.024 .

De Hoog, J.C.M., K. Hattori, and H. Jung. 2014. Titanium- and water-rich metamorphic olivine in high-pressure serpentinites from the Voltri Massif (Ligurian Alps, Italy): evidence for deep subduction of high-field strength and fluid-mobile elements. *Contributions to Mineralogy and Petrology 167*(3): 990. https://doi.org/10.1007/s00410-014-0990-x .

De Hoog, J.C.M. and I.P. Savov. 2018. Boron Isotopes as a Tracer of Subduction Zone Processes, In *Boron Isotopes: The Fifth Element*, eds. Marschall, H. and G. Foster, Advances in Isotope Geochemistry, 217–247. Cham: Springer International Publishing. https://doi.org/10.1007/978-3-319-64666-4_9.

Debret, B., K.T. Koga, F. Cattani, C. Nicollet, G. Van den Bleeken, and S. Schwartz. 2016. Volatile (Li, B, F and Cl) mobility during amphibole breakdown in subduction zones. *Lithos* 244: 165–181. https://doi.org/10.1016/j.lithos.2015.12.004 .

Demény, A., Z.D. Sharp, and H.R. Pfeifer. 1997. Mg-metasomatism and formation conditions of Mg-chlorite-muscovite-quartzphyllites (leucophyllites) of the Eastern Alps (W. Hungary) and their relations to Alpine whiteschists. *Contributions to Mineralogy and Petrology 128*(2): 247–260. https://doi.org/10.1007/s004100050306 .

Di Vincenzo, G., S. Tonarini, B. Lombardo, D. Castelli, and L. Ottolini. 2006. Comparison of 40Ar–39Ar and Rb–Sr Data on Phengites from the UHP Brossasco–Isasca Unit (Dora Maira Massif, Italy): Implications for Dating White Mica. *Journal of Petrology 47*(7): 1439–1465. https://doi.org/10.1093/petrology/egl018 .

Dyar, M.D., M. Wiedenbeck, D. Robertson, L.R. Cross, J.S. Delaney, K. Ferguson, C.A. Francis, E.S. Grew, C.V. Guidotti, R.L. Hervig, J.M. Hughes, J. Husler, W. Leeman, A.V. McGuire, D. Rhede, H. Rothe, R.L. Paul, I. Richards, and M. Yates. 2001. Reference Minerals for the Microanalysis of Light Elements. *Geostandards Newsletter 25*(2-3): 441–463. https://doi.org/10.1111/j.1751-908X.2001.tb00616.x .

Ferrando, S. 2012. Mg-metasomatism of metagranitoids from the Alps: genesis and possible tectonic scenarios. *Terra Nova 24*(6): 423–436. https://doi.org/10.1111/j.1365-3121.2012.01078.x .

Ferrando, S., M.L. Frezzotti, M. Petrelli, and R. Compagnoni. 2009. Metasomatism of continental crust during subduction: the UHP whiteschists from the Southern Dora-Maira Massif (Italian Western Alps). *Journal of Metamorphic Geology 27*(9): 739–756. https://doi.org/10.1111/j.1525-1314.2009.00837.x .

Ferrando, S., C. Groppo, M.L. Frezzotti, D. Castelli, and A. Proyer. 2017. Dissolving dolomite in a stable UHP mineral assemblage: Evidence from Cal-Dol marbles of the Dora-Maira Massif (Italian Western Alps). *American Mineralogist 102*(1): 42–60. https://doi.org/10.2138/am-2017-5761 .

Ferraris, C., D. Castelli, and B. Lombardo. 2005. SEM/TEM-AEM characterization of micro- and nano-scale zonation in phengite from a UHP Dora-Maira marble petrologic significance of armoured Si-rich domains. *European Journal of Mineralogy 17*(3): 453–464. https://doi.org/10.1127/0935-1221/2005/0017-0453 .

Galvez, M.E., J.A.D. Connolly, and C.E. Manning. 2016. Implications for metal and volatile cycles from the pH of subduction zone fluids. *Nature 539*(7629): 420–424. https://doi.org/10.1038/nature20103 .

Gauthiez-Putallaz, L., D. Rubatto, and J. Hermann. 2016. Dating prograde fluid pulses during subduction by in situ U–Pb and oxygen isotope analysis. *Contributions to Mineralogy and Petrology 171*(2): 15. https://doi.org/10.1007/s00410-015-1226-4 .

Gebauer, D., H.P. Schertl, M. Brix, and W. Schreyer. 1997. 35 Ma old ultrahigh-pressure metamorphism and evidence for very rapid exhumation in the Dora Maira Massif, Western Alps. *Lithos 41*(1): 5–24. https://doi.org/10.1016/S0024-4937(97)82002-6 .

Groppo, C., D. Castelli, and F. Rolfo. 2007. HT, pre-Alpine relics in a spinel-bearing dolomite marble from the UHP Brossasco-Isasca Unit (Dora-Maira Massif, western Alps, Italy). *Periodico di Mineralogia* 76: 155–168. https://doi.org/10.2451/2007PM0022 .

Groppo, C., S. Ferrando, M. Gilio, S. Botta, F. Nosenzo, G. Balestro, A. Festa, and F. Rolfo. 2019. What's in the sandwich? New P–T constraints for the (U)HP nappe stack of southern Dora-Maira Massif (Western Alps). *European Journal of Mineralogy 31*(4): 665–683. https://doi.org/10.1127/ejm/2019/0031-2860 .

Groppo, C., B. Lombardo, D. Castelli, and P. Cadoppi 2005. Decompressional P-T Path in the Albite-Stability Field of Orthogneiss from the Uhp Unit of the Dora-Maira Massif. In *Abstracts*, Graz.

Groppo, C., B. Lombardo, D. Castelli, and R. Compagnoni. 2007. Exhumation History of the UHPM Brossasco-Isasca Unit, Dora-Maira Massif, as Inferred from a Phengite-Amphibole Eclogite. *International Geology Review 49*(2): 142–168. https://doi.org/10.2747/0020-6814.49.2.142 .

Halama, R., M. Konrad-Schmolke, and J.C.M. De Hoog. 2020. Boron isotope record of peak metamorphic ultrahigh-pressure and retrograde fluid–rock interaction in white mica (Lago di Cignana, Western Alps). *Contributions to Mineralogy and Petrology 175*(3): 20. https://doi.org/10.1007/s00410-020-1661-8 .

Harris, B.J.R., J.C.M. de Hoog, and R. Halama. 2022. The behaviour of nitrogen during subduction of oceanic crust: Insights from in situ SIMS analyses of high-pressure rocks. *Geochimica et Cosmochimica Acta* 321: 16–34. https://doi.org/10.1016/j.gca.2022.01.018 .

Harvey, J., C.J. Garrido, I. Savov, S. Agostini, J.A. Padrón-Navarta, C. Marchesi, V. López Sánchez-Vizcaíno, and M.T. Gómez-Pugnaire. 2014. 11B-rich fluids in subduction zones: The role of antigorite dehydration in subducting slabs and boron isotope heterogeneity in the mantle. *Chemical Geology* 376:

20–30. https://doi.org/10.1016/j.chemgeo.2014.03.015 .

Hermann, J. 2003. Experimental evidence for diamond-facies metamorphism in the Dora-Maira massif. *Lithos 70*(3): 163–182. https://doi.org/10.1016/S0024-4937(03)00097-5 .

Herviou, C., A. Verlaguet, P. Agard, M. Locatelli, H. Raimbourg, B. Lefeuvre, and B. Dubacq. 2021. Along-dip variations of subduction fluids: The 30–80 km depth traverse of the Schistes Lustrés complex (Queyras-Monviso, W. Alps). *Lithos* 394-395: 106168. https://doi.org/10.1016/j.lithos.2021.106168 .

Hughes, L., S. Cuthbert, A. Quas-Cohen, L. Ruzié-Hamilton, A. Pawley, G. Droop, I. Lyon, R. Tartèse, and R. Burgess. 2021. Halogens in Eclogite Facies Minerals from the Western Gneiss Region, Norway. *Minerals 11*(7): 760. https://doi.org/10.3390/min11070760 .

Ishikawa, T. and E. Nakamura. 1993. Boron isotope systematics of marine sediments. *Earth and Planetary Science Letters 117*(3): 567–580. https://doi.org/10.1016/0012-821X(93)90103-G .

Jochum, K.P. and B. Stoll. 2008. Reference materials for elemental and isotopic analyses by LA-(MC)-ICP-MS: Successes and outstanding needs. *Laser Ablation ICP-MS in the Earth Sciences: Current practices and outstanding issues* 40: 147–168 .

Johnson, B. and C. Goldblatt. 2015. The nitrogen budget of Earth. *Earth-Science Reviews* 148: 150–173. https://doi.org/10.1016/j.earscirev.2015.05.006 .

Klemme, S., H.R. Marschall, D.E. Jacob, S. Prowatke, and T. Ludwig. 2011. Trace-element partitioning and boron isotope fractionation between white mica and tourmaline. *The Canadian Mineralogist 49*(1): 165–176. https://doi.org/10.3749/canmin.49.1.165 .

Konrad-Schmolke, M. and R. Halama. 2014. Combined thermodynamic–geochemical modeling in metamorphic geology: Boron as tracer of fluid–rock interaction. *Lithos* 208-209: 393–414. https://doi.org/10.1016/j.lithos.2014.09.021 .

Konrad-Schmolke, M., R. Halama, and V.C. Manea. 2016. Slab mantle dehydrates beneath Kamchatka—Yet recycles water into the deep mantle. *Geochemistry, Geophysics, Geosystems 17*(8): 2987–3007. https://doi.org/10.1002/2016GC006335 .

Kowalski, P.M., B. Wunder, and S. Jahn. 2013. Ab initio prediction of equilibrium boron isotope fractionation between minerals and aqueous fluids at high P and T. *Geochimica et Cosmochimica Acta* 101: 285–301. https://doi.org/10.1016/j.gca.2012.10.007 .

Lardeaux, J.M., S. Schwartz, P. Tricart, A. Paul, S. Guillot, N. Béthoux, and F. Masson. 2006. A crustal-scale cross-section of the south-western Alps combining geophysical and geological imagery. *Terra Nova 18*(6): 412–422. https://doi.org/10.1111/j.1365-3121.2006.00706.x .

Luisier, C., L.P. Baumgartner, B. Putlitz, and T. Vennemann. 2021. Whiteschist genesis through metasomatism and metamorphism in the Monte Rosa nappe (Western Alps). *Contributions to Mineralogy and Petrology 176*(1): 10. https://doi.org/10.1007/s00410-020-01759-0 .

Maffeis, A., S. Ferrando, J.A.D. Connolly, C. Groppo, M.L. Frezzotti, and D. Castelli. 2021. Thermodynamic analysis of HP-UHP fluid inclusions: The solute load and chemistry of metamorphic fluids. *Geochimica et Cosmochimica Acta* 315: 207–229. https://doi.org/10.1016/j.gca.2021.08.044 .

Manning, C.E. 2004. The chemistry of subduction-zone fluids. *Earth and Planetary Science Letters 223*(1): 1–16. https://doi.org/10.1016/j.epsl.2004.04.030 .

Marger, K., C. Luisier, L.P. Baumgartner, B. Putlitz, B.L. Dutrow, A.S. Bouvier, and A. Dini. 2019. Origin of Monte Rosa whiteschist from in-situ tourmaline and quartz oxygen isotope analysis by SIMS using new tourmaline reference materials. *American Mineralogist 104*(10): 1503–1520. https://doi.org/10.2138/am-2019-7012 .

Marschall, H.R. 2018. Boron Isotopes in the Ocean Floor Realm and the Mantle, In *Boron Isotopes: The Fifth Element*, eds. Marschall, H. and G. Foster, Advances in Isotope Geochemistry, 189–215. Cham: Springer International Publishing. https://doi.org/10.1007/978-3-319-64666-4_8.

Marschall, H.R., R. Altherr, T. Ludwig, A. Kalt, K. Gméling, and Z. Kasztovszky. 2006. Partitioning and budget of Li, Be and B in high-pressure metamorphic rocks. *Geochimica et Cosmochimica Acta 70*(18): 4750–4769. https://doi.org/10.1016/j.gca.2006.07.006 .

Marschall, H.R., R. Altherr, and L. Rüpke. 2007. Squeezing out the slab — modelling the release of Li, Be and B during progressive high-pressure metamorphism. *Chemical Geology 239*(3): 323–335. https://doi.org/10.1016/j.chemgeo.2006.08.008 .

Marschall, H.R., T. Ludwig, R. Altherr, A. Kalt, and S. Tonarini. 2006. Syros Metasomatic Tourmaline: Evidence for Very High-δ^{11}B Fluids in Subduction Zones. *Journal of Petrology 47*(10): 1915–1942. https://doi.org/10.1093/petrology/egl031 .

Marschall, H.R., V.D. Wanless, N. Shimizu, P.A.E. Pogge von Strandmann, T. Elliott, and B.D. Monteleone. 2017. The boron and lithium isotopic composition of mid-ocean ridge basalts and the mantle. *Geochimica et Cosmochimica Acta* 207: 102–138. https://doi.org/10.1016/j.gca.2017.03.028 .

Martin, C., K.E. Flores, A. Vitale-Brovarone, S. Angiboust, and G.E. Harlow. 2020. Deep mantle serpentinization in subduction zones: Insight from in situ B isotopes in slab and mantle wedge serpentinites. *Chemical Geology* 545: 119637. https://doi.org/10.1016/j.chemgeo.2020.119637 .

Martin, C., E. Ponzevera, and G. Harlow. 2015. In situ lithium and boron isotope determinations in mica, pyroxene, and serpentine by LA-MC-ICP-MS. *Chemical Geology* 412: 107–116. https://doi.org/10.1016/j.chemgeo.2015.07.022 .

Morgan, G.B. and D. London. 1989. Experimental reactions of amphibolite with boron-bearing aqueous fluids at 200 MPa: implications for tourmaline stability and partial melting in mafic rocks. *Contributions to Mineralogy and Petrology 102*(3): 281–297. https://doi.org/10.1007/BF00373721 .

Nowlan, E.U., H.P. Schertl, and W. Schreyer. 2000. Garnet–omphacite–phengite thermobarometry of eclogites from the coesite-bearing unit of the southern Dora-Maira Massif, Western Alps. *Lithos 52*(1): 197–214. https://doi.org/10.1016/S0024-4937(99)00091-2 .

Pabst, S., T. Zack, I.P. Savov, T. Ludwig, D. Rost, S. Tonarini, and E.P. Vicenzi. 2012. The fate of subducted oceanic slabs in the shallow mantle: Insights from boron isotopes and light element composition of metasomatized blueschists from the Mariana forearc. *Lithos* 132-133: 162–179. https://doi.org/10.1016/j.lithos.2011.11.010 .

Padrón-Navarta, J.A., V.L. Sánchez-Vizcaíno, J. Hermann, J.A.D. Connolly, C.J. Garrido, M.T. Gómez-Pugnaire, and C. Marchesi. 2013. Tschermak's substitution in antigorite and consequences for phase relations and water liberation in high-grade serpentinites. *Lithos* 178: 186–196. https://doi.org/10.1016/j.lithos.2013.02.001 .

Pawlig, S. and L.P. Baumgartner. 2001. Geochemistry of a talc-kyanite-chloritoid shear zone within the Monte Rosa granite, Val d'Ayas, Italy. *Schweizerische Mineralogische und Petrographische Mitteilungen* 81: 329–346. https://doi.org/10.5169/seals-61696 .

Peacock, S.M. and R.L. Hervig. 1999. Boron isotopic composition of subduction-zone metamorphic rocks. *Chemical Geology 160*(4): 281–290. https://doi.org/10.1016/S0009-2541(99)00103-5 .

Penniston-Dorland, S.C., S.S. Sorensen, R.D. Ash, and S.V. Khadke. 2010. Lithium isotopes as a tracer of fluids in a subduction zone mélange: Franciscan Complex, CA. *Earth and Planetary Science Letters 292*(1): 181–190. https://doi.org/10.1016/j.epsl.2010.01.034 .

Philippot, P., P. Chevallier, C. Chopin, and J. Dubessy. 1995. Fluid composition and evolution in coesite-bearing rocks (Dora-Maira massif, Western Alps): implications for element recycling during subduction. *Contributions to Mineralogy and Petrology 121*(1): 29. https://doi.org/10.1007/

s004100050088 .

Plank, T. 2014. The Chemical Composition of Subducting Sediments, In *Treatise on Geochemistry (Second Edition)*, eds. Holland, H.D. and K.K. Turekian, 607–629. Oxford: Elsevier. https://doi.org/10.1016/B978-0-08-095975-7.00319-3.

Rubatto, D. 2017. Zircon: The Metamorphic Mineral. *Reviews in Mineralogy and Geochemistry 83*(1): 261–295. https://doi.org/10.2138/rmg.2017.83.9 .

Rubatto, D. and J. Hermann. 2001. Exhumation as fast as subduction? *Geology 29*(1): 3–6. https://doi.org/10.1130/0091-7613(2001)029⟨0003:EAFAS⟩2.0.CO;2 .

Scambelluri, M., O. Müntener, L. Ottolini, T.T. Pettke, and R. Vannucci. 2004. The fate of B, Cl and Li in the subducted oceanic mantle and in the antigorite breakdown fluids. *Earth and Planetary Science Letters 222*(1): 217–234. https://doi.org/10.1016/j.epsl.2004.02.012 .

Schertl, H.P. and W. Schreyer. 2008. Geochemistry of coesite-bearing pyrope quartzite and related rocks from the Dora-Maira Massif, Western Alps. *Eur.J.Mineral.* 20: 791–809. https://doi.org/10.1127/0935-1221/2008/0020-1862 .

Schertl, H.P., W. Schreyer, and C. Chopin. 1991. The pyrope-coesite rocks and their country rocks at Parigi, Dora Maira Massif, Western Alps: detailed petrography, mineral chemistry and PT-path. *Contributions to Mineralogy and Petrology 108*(1): 1–21. https://doi.org/10.1007/BF00307322 .

Schreyer, W. 1973. Whiteschist: A High-Pressure Rock and its Geologic Significance. *The Journal of Geology 81*(6): 735–739. https://doi.org/10.1086/

627926 .

Sharp, Z.D. and J.D. Barnes. 2004. Water-soluble chlorides in massive seafloor serpentinites: a source of chloride in subduction zones. *Earth and Planetary Science Letters 226*(1): 243–254. https://doi.org/10.1016/j.epsl.2004.06.016 .

Sharp, Z.D., E.J. Essene, and J.C. Hunziker. 1993. Stable isotope geochemistry and phase equilibria of coesite-bearing whiteschists, Dora Maira Massif, western Alps. *Contributions to Mineralogy and Petrology 114*(1): 1–12. https://doi.org/10.1007/BF00307861 .

Sievers, N.E., C.A. Menold, M. Grove, and M.A. Coble. 2017. White mica trace element and boron isotope evidence for distinctive infiltration events during exhumation of deeply subducted continental crust. *International Geology Review 59*(5-6): 621–638. https://doi.org/10.1080/00206814.2016.1219881 .

Simon, G., C. Chopin, and V. Schenk. 1997. Near-end-member magnesiochloritoid in prograde-zoned pyrope, Dora-Maira massif, western Alps. *Lithos 41*(1): 37–57. https://doi.org/10.1016/S0024-4937(97)82004-X .

Smith, H.J., A.J. Spivack, H. Staudigel, and S.R. Hart. 1995. The boron isotopic composition of altered oceanic crust. *Chemical Geology 126*(2): 119–135. https://doi.org/10.1016/0009-2541(95)00113-6 .

Sorensen, J.N. Grossman, and M.R. Perfit. 1997. Phengite-hosted LILE Enrichment in Eclogite and Related Rocks: Implications for Fluid-Mediated Mass Transfer in Subduction Zones and Arc Magma Genesis. *Journal of Petrology 38*(1): 3–34. https://doi.org/10.1093/petroj/38.1.3 .

Svensen, H., B. Jamtveit, D.A. Banks, and H. Austrheim. 2001. Halogen contents of eclogite facies fluid inclusions and minerals: Caledonides, western Norway. *Journal of Metamorphic Geology 19*(2): 165–178. https://doi.org/10.1046/j.0263-4929.2000.00301.x .

Tian, Y., Y. Xiao, Y.X. Chen, H. Sun, H. Liu, F. Tong, J.H. Yang, and H.P. Schertl. 2019. Serpentinite-derived low δ^7Li fluids in continental subduction zones: Constraints from the fluid metasomatic rocks (whiteschist) from the Dora-Maira Massif, Western Alps. *Lithos* 348-349: 105177. https://doi.org/10.1016/j.lithos.2019.105177 .

Tonarini, S., W.P. Leeman, and P.T. Leat. 2011. Subduction erosion of forearc mantle wedge implicated in the genesis of the South Sandwich Island (SSI) arc: Evidence from boron isotope systematics. *Earth and Planetary Science Letters 301*(1): 275–284. https://doi.org/10.1016/j.epsl.2010.11.008 .

Ulmer, P. and V. Trommsdorff. 1995. Serpentine Stability to Mantle Depths and Subduction-Related Magmatism. *Science 268*(5212): 858–861. https://doi.org/10.1126/science.268.5212.858 .

Urann, B.M., V.L. Roux, T. John, G.M. Beaudoin, and J.D. Barnes. 2020. The distribution and abundance of halogens in eclogites: An in situ SIMS perspective of the Raspas Complex (Ecuador). *American Mineralogist 105*(3): 307–318. https://doi.org/10.2138/am-2020-6994 .

Walowski, K.J., L.A. Kirstein, J.C.M. De Hoog, T.R. Elliott, I.P. Savov, and R.E. Jones. 2019. Investigating ocean island mantle source heterogeneity with boron isotopes in melt inclusions. *Earth and Planetary Science Letters* 508: 97–108. https://doi.org/10.1016/j.epsl.2018.12.005 .

Whitney, D.L. and B.W. Evans. 2010. Abbreviations for names of rock-forming minerals. *American Mineralogist 95*(1): 185–187. https://doi.org/10.2138/am.2010.3371 .

Wunder, B., A. Meixner, R.L. Romer, R. Wirth, and W. Heinrich. 2005. The geochemical cycle of boron: Constraints from boron isotope partitioning experiments between mica and fluid. *Lithos 84*(3): 206–216. https://doi.org/10.1016/j.lithos.2005.02.003 .

Xiong, J.W., Y.X. Chen, H.Z. Ma, H.P. Schertl, Y.F. Zheng, and K.D. Zhao. 2022. Tourmaline boron isotopes trace metasomatism by serpentinite-derived fluid in continental subduction zone. *Geochimica et Cosmochimica Acta* 320: 122–142. https://doi.org/10.1016/j.gca.2022.01.003 .

Xiong, J.W., Y.X. Chen, K. Zhou, H.P. Schertl, Y.F. Zheng, F. Huang, X.P. Xia, and Z.W. Chen. 2021. Fe and O isotopes in coesite-bearing jadeite quartzite from the Western Alps record multistage fluid-rock interactions in a continental subduction zone. *Geochimica et Cosmochimica Acta* 312: 1–24. https://doi.org/10.1016/j.gca.2021.08.006 .

Yamada, C., T. Tsujimori, Q. Chang, and J.I. Kimura. 2019. Boron isotope variations of Franciscan serpentinites, northern California. *Lithos* 334-335: 180–189. https://doi.org/10.1016/j.lithos.2019.02.004 .

Yamaoka, K., T. Ishikawa, O. Matsubaya, D. Ishiyama, K. Nagaishi, Y. Hiroyasu, H. Chiba, and H. Kawahata. 2012. Boron and oxygen isotope systematics for a complete section of oceanic crustal rocks in the Oman ophiolite. *Geochimica et Cosmochimica Acta* 84: 543–559. https://doi.org/10.1016/j.gca.2012.01.043 .

Online resource 1

Online resource 2

Click here to access/download

Electronic supplementary material

OR_2.xlsx

Online resource 3